NREL National Renewable Energy Laboratory

Innovation for Our Energy Future

Characterization of Amorphous Silicon Advanced Materials and PV Devices

Final Technical Report
15 December 2001–31 January 2005

P.C. Taylor
University of Utah
Salt Lake City, Utah

Characterization of Amorphous Silicon Advanced Materials and PV Devices

Final Technical Report
15 December 2001–31 January 2005

P.C. Taylor
University of Utah
Salt Lake City, Utah

NREL Technical Monitor: B. von Roedern

Available electronically at http://www.osti.gov/bridge

Available for a processing fee to U.S. Department of Energy
and its contractors, in paper, from:
      U.S. Department of Energy
      Office of Scientific and Technical Information
      P.O. Box 62
      Oak Ridge, TN 37831-0062
      phone: 865.576.8401
      fax: 865.576.5728
      email: mailto:reports@adonis.osti.gov

Available for sale to the public, in paper, from:
      U.S. Department of Commerce
      National Technical Information Service
      5285 Port Royal Road
      Springfield, VA 22161
      phone: 800.553.6847
      fax: 703.605.6900
      email: orders@ntis.fedworld.gov
      online ordering: http://www.ntis.gov/ordering.htm

Printed on paper containing at least 50% wastepaper, including 20% postconsumer waste

Table of Contents

List of Figures

1. INTRODUCTION

Objectives

The major objectives of this subcontract have been (1) to understand the microscopic properties of the defects that contribute to the Staebler-Wronski effect in order to eliminate this effect, (2) to perform correlated studies on films and devices made by novel techniques, especially those with promise to improve stability or deposition rates, (3) to understand the structural, electronic and optical properties of films of hydrogenated amorphous silicon (a-Si:H) made on the boundary between the amorphous and microcrystalline phases, (4) to search for more stable intrinsic layers of a-Si:H, (5) to characterize the important defects, impurities, and metastabilities in the bulk and at surfaces and interfaces in a-Si:H films and devices and in important alloy systems, and (6) to make state-of-the-art plasma enhanced chemical vapor deposition (PECVD) devices out of new, advanced materials when appropriate. All of these goals are highly relevant to the improvement of photovoltaic (PV) devices based on a-Si:H and related alloys. With regard to the first objective, we have identified a paired hydrogen site that may be the defect that stabilizes the silicon dangling bonds formed in the Staebler-Wronski effect.

Approaches

In this subcontract we have emphasized two approaches that are unique to the research group at Utah. First, we have used novel electron paramagnetic (or spin) resonance (ESR) and nuclear magnetic resonance (NMR) techniques, such as measurements of silicon dangling bonds using second harmonic detection of ESR and measurements of the spin-lattice relaxation in a dipolar field (T_{1D}) or in a rotating frame ($T_{1\rho}$) to probe the influence of paramagnetic silicon dangling bonds in doped and intrinsic a-Si:H and selected alloys. The research group at Utah has pioneered the development of these two techniques as applied to amorphous semiconductors. Our experiments have given a better microscopic understanding of metastabilities in a-Si:H and related alloys. Second, we have used below-gap optical spectroscopy [photoluminescence (PL), PL excitation (PLE), ESR, optical absorption, optically detected magnetic resonance (ODMR), etc.] with a tunable Ti sapphire laser system to excite carriers at energies that extend from above the optical gap to well below the gap (down to ~ 0.1 eV).

We have also performed more standard experiments, such as photothermal deflection spectroscopy (PDS) and the constant photocurrent method (CPM) to measure absorption, ESR to measure defect densities, NMR to look at clustered and dilute hydrogen, and PL to measure material quality.

Research Tasks

The subcontract is divided into three tasks. One task has been the growth and characterization of a-Si:H and related alloys. For this task we have used our three-chamber system PECVD system, which is capable of making state-of-the-art films and devices. For the

characterization of a-Si:H and related alloys we have used photoconductivity (PC), PLE ESR, and optically induced (light induced) ESR (LESR). A second task has been the characterization of films of a-Si:H grown at the amorphous microcrystalline boundary. We have studied the morphology of microcrystalline films using atomic force microscopy (AFM) [see publication 2] and the defects using ESR [see publications 5, 12, 13]. A third task has been to characterize material properties of films used in actual devices. We have completed our studies of the stability of cells made using silicon-sulfur alloys for the intrinsic layer [see publication 10]. Also, we have compared defects measured by ESR with defects measured by CPM in PV devices made at Pennsylvania State University [see publication 22]. These comparisons confirm the presence of two distinct defects involved in the Staebler-Wronski effect but have not yet identified which defect measured by CPM corresponds to the one measured by ESR. A fourth task has been to measure defects, impurities and metastabilities in a-Si:H and related alloys. Second harmonic detection of LESR has been employed to measure the universal decays of band-tail electrons and holes in a-Si:H [see publications 3,4,6,8,16] and a-Ge:H [see publication 7]. The Staebler-Wronski effect has been observed for the first time in a-Ge:H using ESR [see publications 19 and 20]. Investigations of the optically induced production of silicon dangling bonds in a-Si:H at low temperatures have been completed [see publication 14]. In addition, the role of a metastable paired hydrogen defect (H doublet) has been investigated using NMR in samples of a-Si:H grown by PECVD, with and without hydrogen dilution. This hydrogen doublet is probably the defect responsible for stabilizing the silicon dangling bonds that are produced in the Staebler-Wronski effect [see publications 9, 15, 17, 18]. Initial theoretical calculations [see publication 23] are consistent with the site being a specific type of dihydride bonding (SiH_2) site. In addition, we have initiated a novel way of looking at defect generation in a-Si:H, namely the production of silicon dangling bonds by decay of tritium (^3H), which is bonded to silicon [see publication 21]. The tritium decays to helium, which does not bond to Si. Finally, PL from Er^{3+} in partially crystalline a-Si:H has been measured [see publication 1]. A review of some of the earlier work performed under this sub-contract is also available [publication 11].

Results

The most significant results of the three phases of the sub-contract are (1) the discovery of a paired hydrogen site in light-soaked a-Si:H that is probably the stabilization mechanism for the silicon dangling bonds created in the Staebler-Wronski effect, (2) the confirmation of universal kinetics for the decay of optically excited electrons and holes in a-Si:H and a-Ge:H at low temperatures, (3) the first detection of the Staebler-Wronski effect in a-Ge:H, (4) the use of a novel decay of tritium in a-Si:H to probe the production of silicon dangling-bond defects, and (5) the comparison of ESR and CPM measurements of defects in a-Si:H material used in cells.

2. A PAIRED HYDROGEN SITE AND THE STAEBLER-WRONSKI EFFECT IN a-Si:H

Our studies of NMR in light soaked samples of a-Si:H have provided evidence that a specific hydrogen-related defect is linked to the Staebler-Wronski effect. The interaction between hydrogen impurities and defects in crystalline and amorphous solids is of general interest in many diverse materials systems. In crystalline semiconductors, such as silicon [1] for example, hydrogen can passivate dopants, assist in the diffusion of impurities, generate

metastable defects such as H_2^*, [2] and aggregate along selected planes to produce "platelets" [3]. Therefore, understanding the role of hydrogen in the production of the defects that produce the Staebler-Wronski effect [4] in a-Si:H is essential in providing a general understanding of the role of hydrogen in mediating metastabilities in a wide class of materials.

In a-Si:H, hydrogen has long been implicated in the Staebler-Wronski effect [4], which is characterized by a decrease in both the dark and photoconductivities after irradiation with visible light. These decreases are attributed to the production of approximately 10^{17} cm^{-3} of silicon dangling bonds, which are defects that serve as non-radiative recombination centers for carriers. Although hydrogen has long been implicated as contributing to the Staebler-Wronski effect, no direct microscopic evidence exists to confirm this suspicion. We have found the first direct evidence for optically induced changes in the local environment of a subset of the hydrogen atoms *at densities comparable* to those of the silicon dangling bonds that contribute to the Staebler-Wronski effect. After optical excitation, the nuclear magnetic resonance (NMR) of ^{1}H exhibits a hydrogen "doublet" that corresponds to a site with two hydrogen atoms spaced approximately 2.3 Å apart. This hydrogen "defect", whose density is between 10^{17} and 10^{18} cm^{-3}, can be thermally annealed with kinetics that generally match the annealing of the silicon dangling bonds.

The film of a-Si:H employed in the study was made in a large area deposition system at BPSolar by DC plasma enhanced chemical vapor deposition (PECVD) of silane (SiH$_4$). The pressure in the reactor was 0.5 Torr; the power density was ~50 mW/cm^2; and the substrate temperature was ~200 C. These conditions represent those used in standard photovoltaic devices for which the electronic and optical properties are very well known. The film was deposited on Al foil and half of the area was irradiated with a solar simulator for 600 hr (light-soaked sample). Two NMR samples were made from the irradiated and un-irradiated areas by dissolving away the Al foils in dilute hydrochloric acid and placing the cleaned powders in quartz tubes. The NMR measurements were made at 7 K using a standard pulsed spectrometer.[5] The stimulated echo from a Jeener-Broekaert three-pulse sequence was employed to measure the ^{1}H NMR signals [5]. Samples were annealed in a nitrogen environment at 160 and 200 C.

Figure 1 show the Fourier transform of the stimulated dipolar echo, which represents the lineshape in frequency space, in the two samples of a-Si:H measured under various conditions. [We show the real transforms in Fig. 1 to improve the signal-to-noise ratios and eliminate small phase errors due to long term drift during signal averaging. The complex transforms exhibit the same features with slight asymmetries in the line shapes.] The bottom trace (d) is the lineshape of that portion of the sample that was not exposed to light (as-grown sample). This lineshape contains the two standard features, a narrow Lorentzian line attributed to hydrogen bonded to silicon atoms in a dilute (essentially random) configuration and a broad Gaussian line attributed to hydrogen bonded to silicon in a clustered environment, such as might be obtained on the internal surfaces of microvoids. The top trace (a) is the lineshape in that portion of the sample that was exposed to light (light-soaked sample). In addition to the two standard features, there exist two small peaks separated from the central frequency, which is labeled zero in Fig. 1, by about 8 kHz. [The features at ~23 kHz are artifacts due to an unknown, small interference with the NMR detection signal, which also occurs in the absence of a sample.] The trace just below the top trace (b) is the spectrum in the light-soaked sample after annealing at 170 C for 4 hours.
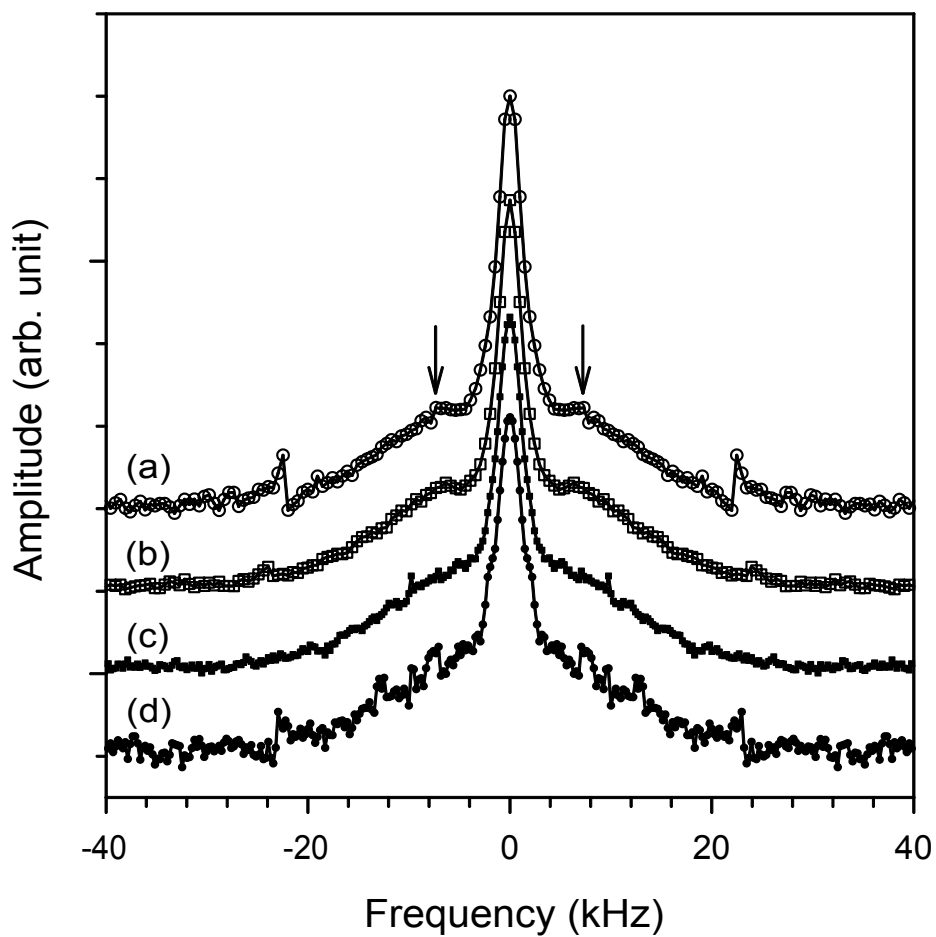
Figure 1. [1]H Jeener-Broekaert stimulated echo spectra in a-Si:H. (a) sample irradiated for 600 hr using a solar simulator; (b) irradiated sample after annealing at 170 C for 4 hours; (c) irradiated sample after annealing at 170 C for 4 hours followed by annealing at 200 C for 4 hours; (d) sample as grown (no irradiation and no annealing). Arrows point to the appearance of a hydrogen doublet in the irradiated sample. The peaks near ∀23 kHz are artifacts.

This procedure is known to anneal the Staebler-Wronski degradation observed in solar cells made from films of this type [6]. The trace below (c) is the spectrum in the light-soaked sample after additional annealing at 200 C for 4 hours. The spectrum taken after annealing at 200 C and the spectrum in the as-grown sample are identical within experimental error.

Two conclusions are easily deduced from the data in Fig. 1. First, an extra feature appears in the ^{1}H NMR lineshape of Fig. 1 after light soaking the sample. Second, this feature disappears after annealing at 200 C. We have thus found a distinct hydrogen site in a-Si:H that appears on light soaking and disappears on annealing.

We have also studied the temperature dependence of this doublet from 7 to 20 K. Above about 10 K the signal disappears in a manner that is consistent with local motion of the hydrogen atoms. Our first ^{1}H NMR measurements shown above were made at a spectrometer frequency of approximately 80 MHZ. To improve our signal-to-noise ratios, we doubled our spectrometer frequency to about 150 MHz. This change has greatly increased the precision with which we can measure the doublet signal. The first measurements at 150 MHz are shown in Fig. 2. This figure displays only the central portion of the NMR spectrum, the portion that contains the "narrow" line attributed to randomly positioned hydrogen atoms that are bonded to silicon atoms. Our preliminary measurements at lower frequencies indicated that there was a subtle change in the lineshape of this narrow line between 7 and 10 K. We have attributed this slight broadening of the narrow line above about 10 K to the contribution of the partially, motionally-narrowed hydrogen doublet that only appears after light soaking. In samples that have not been light soaked or that have been annealed no such change in the narrow line is observed. In Fig. 2 we show the first confirmation that this subtle lineshape change occurs at 150 MHz as well as at 80 MHz.

Next we describe similar effects in samples of a-Si:H made by a technique (hydrogen dilution of silane in a PECVD reactor) that reduces the saturated densities of the hydrogen "doublet" that corresponds to a site with two hydrogen atoms spaced approximately 2.3 Å apart. Although a detailed microscopic picture of this defect remains elusive, the direct tie to hydrogen is a critical first step that places severe constraints on existing microscopic models for the Staebler-Wronski effect.

The hydrogen-diluted films of a-Si:H were made at BP Solar. Except for the hydrogen dilution, the films were grown using the same parameters as mentioned above for the undiluted films in a large area deposition system by DC plasma enhanced chemical vapor deposition of silane (SiH_4) [7]. After measuring the light-soaked state, the samples were annealed in a nitrogen environment.

In Fig. 3 we show the standard ^{1}H NMR lineshape for the hydrogen bonded to silicon in a-Si:H. The Zeeman frequency has been subtracted from this spectrum so that zero represents the NMR response in the absence of any solid-state interactions. The slight positive/negative asymmetry in the figure is an artifact due to phase errors in the Fourier transform of the data. The narrow Lorentzian line, whose full width at half maximum is approximately 3 kHz, is attributed to hydrogen atoms bonded to silicon atoms at random positions in the amorphous
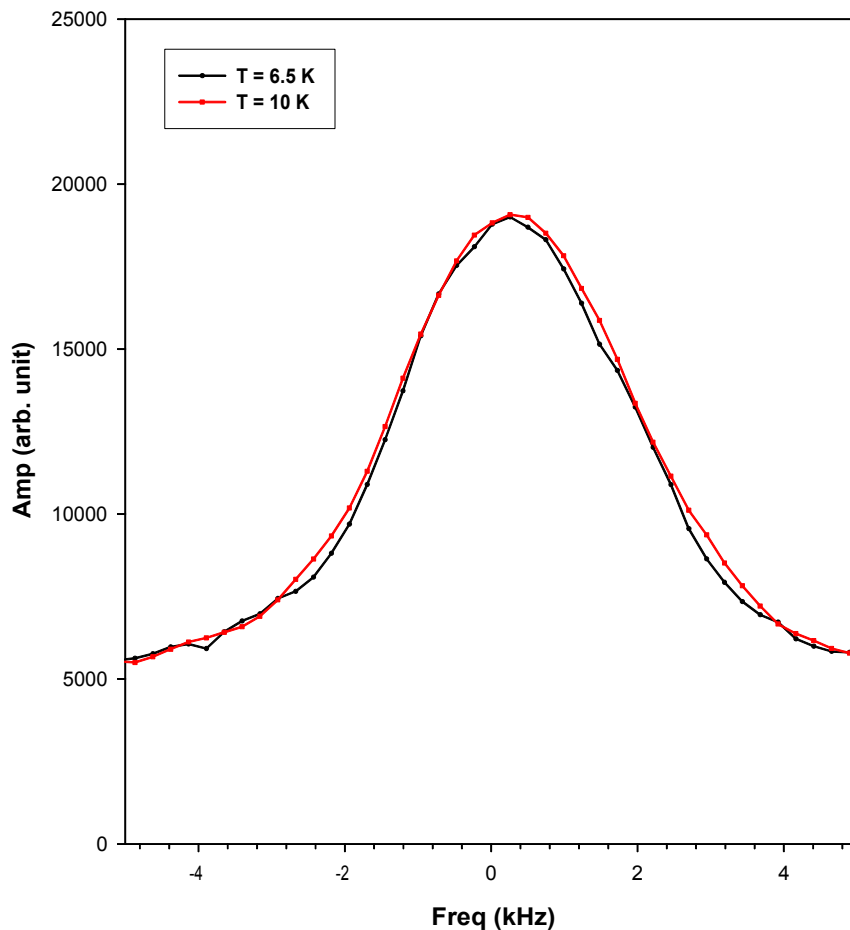
Figure 2. The Fourier transformed spectra of a light-soaked sample of a-Si:H. The black trace is recorded at 8 K. The red trace is from the same sample run at approximately 10 K. The data were taken at a spectrometer frequency of 150 MHz. See text for details.

lattice. The broad line, whose full width at half maximum is approximately 25 kHz, is attributed to hydrogen atoms bonded to silicon atoms in a clustered environment, such as would occur at a "divacancy" or small void in the lattice. The Jeener-Broekaert pulse sequence greatly suppresses these lines.
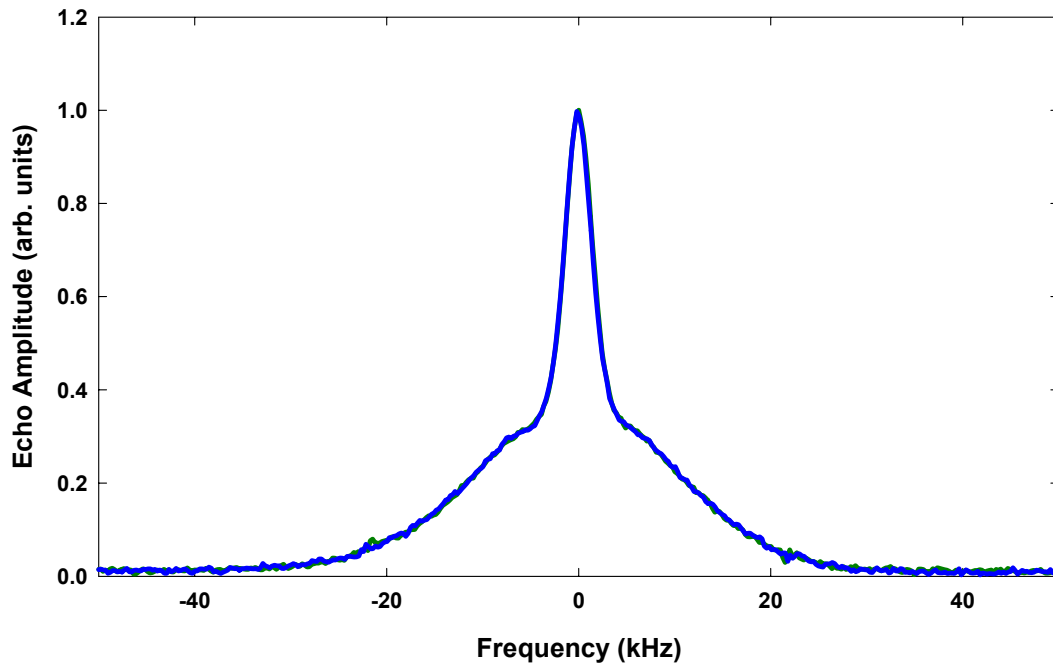
Figure 3. ^{1}H NMR lineshape for hydrogen bonded to silicon in a-Si:H.

For the samples of a-Si:H that were made using hydrogen gas to dilute the silane gas during growth we expect the degradation to be smaller because this procedure is known to decrease the degradation considerably in solar cells. The doublet also appears in these samples after light soaking as shown in Fig. 4. The top trace represents the half of the film that was irradiated in the solar simulator, and the bottom trace represents the unirradiated half of the film. The two arrows indicate the positions of the doublet peaks. As expected the signal-to-noise ratio of the doublet is not as good as in the undiluted sample because the density of doublet sites is smaller by at least a factor of three.

The interaction of the hydrogen doublet sites with the rest of the hydrogen bonded to the silicon lattice is very weak. This fact is determined from measurements of the spin-lattice relaxation rates for the doublet, which are at least an order of magnitude slower that those of the bonded hydrogen below about 7 K [8]. If the doublet sites were closely coupled to the bonded hydrogen, then the rate would follow that of the bonded hydrogen due to rapid spin diffusion. The probable cause for the lack of coupling is that for some reason the doublet sites are physically removed from the bonded hydrogen. Because there are so few doublet sites, the separation may simply be a random occurrence. The temperature dependence of the spin-lattice relaxation rates is also much more rapid than that of the bonded hydrogen. The reason for this anomalous temperature dependence is not known.
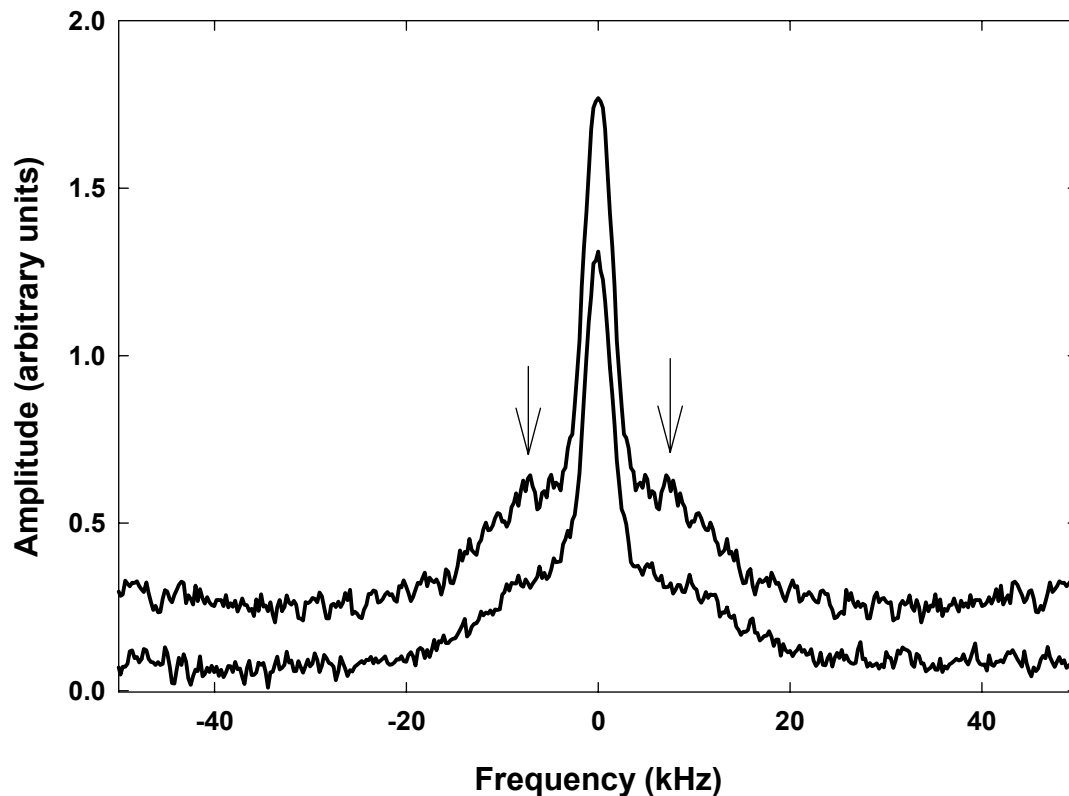
Figure 4. ^{1}H NMR echo line shapes in a hydrogen-diluted sample of a-Si:H before (bottom trace) and after (top trace) irradiation with light. The arrows show the appearance of a paired hydrogen site that appears only after optical excitation. The top trace is displaced vertically for clarity.

Because hydrogen has long been implicated in the Staebler-Wronski effect, many scenarios have been suggested to provide the metastable hydrogen complexes assumed to accompany the light induced production of metastable silicon dangling bonds [7]. We can rule out many of the specific suggestions. First, we can eliminate any models in which the sites do not involve paired hydrogen atoms. Zafar and Schiff [9] first suggested the presence of electrically inactive, paired hydrogen sites, and Branz has also proposed the existence of paired hydrogen sites to explain the optically induced production of metastable silicon dangling bonds [10].

There remain several specific paired-hydrogen sites that are at present consistent with the data. Since the separation between the hydrogen atoms is consistent with SiH_2, or dihydride bonding, one cannot rule out this site as a possibility [7,8]. Several other specific sites have been proposed, including the analog in a-Si:H of the H_2^* defect that occurs in crystalline silicon [11], molecular hydrogen [12], and a surface dimer at a fully hydrogenated multivacancy [13,14]. We can rule out these specific examples because the hydrogen atoms are too far apart, too close together, or too close to bonded hydrogen atoms, respectively.

In addition to the dihydride site, several other specific sites are consistent with the hydrogen-hydrogen separation of 2.3 Å. One site proposed by van de Walle and Tuttle [12], albeit as an intermediate state and not as the stabilizing defect, is a five-fold-coordinated silicon atom with two Si-H bonds. In order for this site to be correct, the stability must somehow be enhanced in the amorphous environment over that which is the case in crystalline Si. Recently, Chadi has suggested two closely spaced Si-H bonds (H_2^{**}) formed by distortion of an H_2^* configuration [11]. It remains to be seen which, if any, of these models is correct.

3. DEFECTS IN HYDROGENATED MICROCRYSTALLINE SILICON

Using the ESR technique, we have made considerable progress on understanding the defects that occur in microcrystalline silicon. The paramagnetic centers in μc-Si:H have been systematically studied since 1994. [15] However, a unique interpretation concerning their microscopic origin has not been established so far. The most relevant signal that is usually observed in the dark ESR of μc-Si:H has a zero crossing g value, g_0, of 2.005, and it is often associated with silicon dangling bonds (DB). Nevertheless, this center has a clear asymmetric line-shape, which is very different from that of Si DBs in a-Si:H. Some authors have attributed this asymmetry to the presence of two different centers [16,17]. One center is supposed to be a Si DB with a g value of 2.0052, while the other ($g_0 = 2.0043$) was initially attributed to electrons trapped in the conduction band tails of the amorphous phase [16]. Another interpretation for the second center is the presence of Si DBs in an oxygen-rich environment [17]. Recently, this signal was explained as a consequence of P_b centers with $g_{\parallel} = 2.0022$ and $g_{\perp} = 2.0078$ [18].
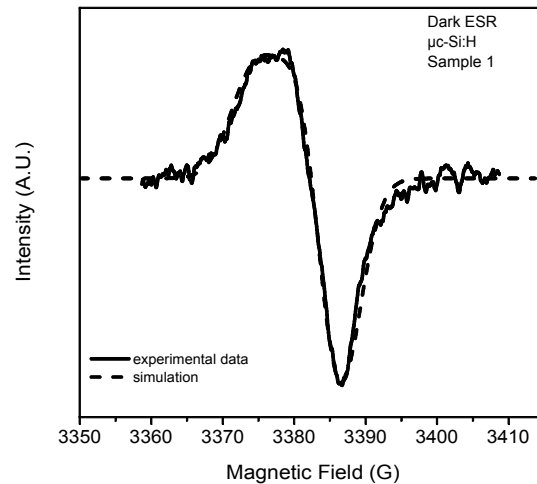

Figure 5. Experimental result and computer simulation of dark ESR in a μc-Si:H sample. The parameters used in the powder pattern simulation are $g_{\parallel} = 2.0096$, $g_{\perp} = 2.0031$ and a Gaussian broadening of 3.2 G.

Another very important signal that occurs in μc-Si:H has $g_0 = 1.998$ and it appears after illumination, for high quality samples. Originally, this line was ascribed to free electrons in the conduction band, since its g_0 is almost the same as that for conduction electrons in crystalline silicon [15]. However, others have attributed the LESR signal to electrons trapped in the localized, conduction band tail states [19,20,21].

The μc-Si:H is a material that shows different morphological structures: 1) (usually) randomly oriented crystalline grains; 2) an amorphous phase; 3) boundaries between the amorphous and crystalline phases; and 4) boundaries between different crystalline grains. In principle, the paramagnetic defects in this material could occur in any of these regions making their identification difficult. In this work, we propose an alternative explanation to the presence of both dark and light-induced ESR signals in μc-Si:H.

Figure 5 shows the experimental dark ESR signal for sample 1. The measurement was performed at room temperature (RT), using 100 μW of microwave power. The asymmetric line shape can be simulated (dotted line) assuming a powder pattern of a single center with $g_{\parallel} = 2.0096$, $g_{\perp} = 2.0031$, and a Gaussian broadening of 3.2 G. The spin density was estimated as about 1×10^{17} cm^{-3}. The dark signal in sample 2 was not studied in detail because it was barely detectable. Sample 2, which consists of four films on quartz substrates, contains much less material, and in addition the dark spin density is much smaller ($\leq 10^{16}$ spins/cm^3) than in sample 1. Finally, because sample 2 is on a quartz substrate, there exists an e' signal on the substrate that is created during the film deposition [22]. This signal partially overlaps the dark spin signal from the μc-Si:H.

The intensity of the dark ESR as a function of microwave power is shown in Fig. 6 for 10 K and room temperature. The straight lines of slope 0.5 represent the unsaturated behavior. At room temperature the signal is not saturated until approximately 1 mW of microwave power. At 10 K, on the other hand, the signal is always saturated, even at very low microwave power, such as 1 μW.

Figure 7 shows the LESR signal for sample 1 (circles) and 2 (crosses) with the dark signal removed by subtraction. Figure 3 also includes a computer simulation (straight line) that is the sum of two different centers: 1) an axially symmetric center powder pattern with $g_{\parallel} = 1.999$ and $g_{\perp} = 1.996$ convoluted with Lorentzian broadening of 3 G; and 2) a center with a g tensor whose symmetric component is $g_0 = 1.998$ convoluted with Gaussian broadening of 8 G. The g-tensor of the second center is assumed to be symmetric for simplicity since the large Gaussian broadening masks any anisotropies in g value. In addition, the intensities of these two centers are assumed to be the same for simplicity. This assumption appears to be roughly correct. No simulation using only a single center fits satisfactorily the experimental curves because of the contrast between the sharp feature at the center and the broad wings.
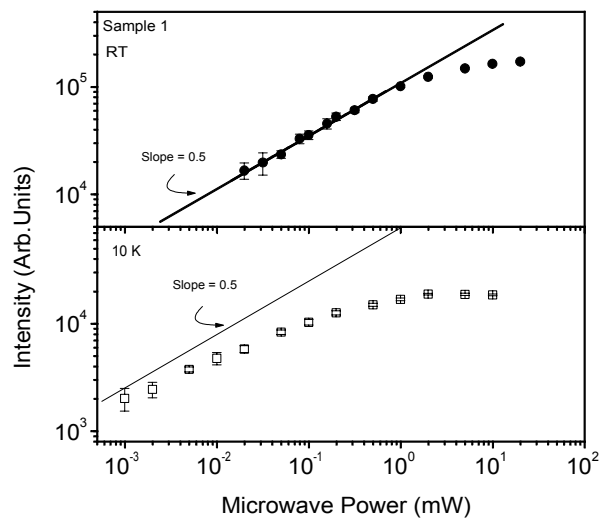
Figure 6. Saturation study for the dark signal in μc-Si:H. At room temperature the signal is not saturated until ~1 mW of microwave power while at 10 K the signal is always saturate

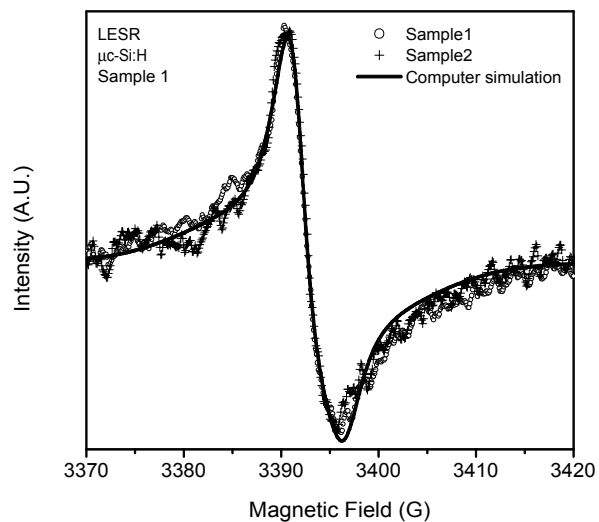**Figure 7.** LESR signal for μc-Si:H measured in two different samples. The straight line is a powder pattern simulation of two centers as discussed in the text.

11

Concerning the ESR signal in the dark, its previous attribution to Si dangling bonds [15,16,23] seems unlikely. First, the spin density measured may be too high to be due only to the small amorphous fraction or to interfaces between crystalline and amorphous silicon. Moreover, because of the hydrogenation, most of the potential silicon dangling bonds should be passivated. Second, the silicon dangling bond in a-Si:H has $g_{\parallel} < g_{\perp}$, [24] which leads to an asymmetry in the line shape opposite to that found in µc-Si:H. Similarly, the P_b center has the wrong asymmetry as compared with the result shown here [18]. Conversely, the g values obtained for µc-Si:H in this work ($g_{\parallel} = 2.0096$ and $g_{\perp} = 2.0031$) are consistent with those reported for charged vacancies in crystalline silicon [25].

However, the attribution of the dark ESR signal to a single, isolated vacancy is not straightforward, since vacancies can combine to form more complex structures such as divacancies [26] or even larger vacancy clusters [27] with different binding energies and annealing temperatures. In crystalline silicon, these defects are usually created by bombardment, and their stability is strongly dependent on temperature [27,28,29]. For instance, the five-vacancy cluster in c-Si, which can be generated by neutron irradiation, is stable at room temperature [27]. Thus, since the µc-Si:H is produced under strong non-equilibrium conditions, it is plausible that the crystalline phase has a relatively high density of stable defects (1×10^{17} cm^{-3}). Of course, a detailed identification of this dark ESR signal of µc-Si:H is very difficult, since there are many possible aggregates of vacancies. Further investigations are needed to refine the microscopic identification of this ESR signal in µc-Si:H.

Another important feature that may help to clarify the origin of the dark ESR signal is its saturation at very low microwave powers at low temperatures. Figure 2 shows clearly that at low temperatures the signal is always saturated at all microwave powers. Even though at low enough microwave power the difference between the intensities due to saturation is only a factor of 2, the changes in the line shape cannot be ignored if one wants to determine properly the g values to compare with well-known centers. In addition, these changes in the line shape due to saturation cannot be used as an indication of the presence of two different centers since another possible explanation for this behavior is the presence of an orientational dependence to the relaxation mechanism or to a change in the g-values with temperature. For instance, in the above-mentioned five-vacancy cluster the changes in the g values with temperature will produce changes in the calculated, powder-pattern line shapes [27].

Regarding the LESR center, it seems to be related with photo-excited carriers trapped in the band tails. The presence of band tail states is a natural consequence of disorder and in µc-Si:H, and they could be related with: 1) strained bonds in the amorphous region; 2) defect states at the grain boundaries between crystalline grains or at crystalline/amorphous interfaces; and in principle, 3) defects or impurities in the crystalline phase. The g values obtained for the LESR center in µc-Si:H are very different from those of optically excited carriers trapped in band-tail states in a-Si:H [30]. Also, the amorphous phase is only a small volume fraction of the film, and its contribution to the ESR and LESR may be unimportant. Of the two remaining possibilities, it is also unlikely that the LESR is due to band-tail states within the crystalline grains themselves. Although charged impurities, such as those that occur in highly doped and compensated Si, can

produce band tails, the level of charged defects (assuming that the dark ESR is due to positively and negatively charged defects) is too small for significant band tailing to occur. Therefore, the LESR in μc-Si:H is probably due to carriers trapped in band-tail states at the grain boundaries between crystalline grains or at crystalline/amorphous interfaces.

Even though the possibility that the LESR signal is due to only a single center cannot be excluded, the results presented here are consistent with the presence of a second signal of equal intensity. Although the identification of these two signals with electrons and holes trapped at the crystalline interface is far from obvious (comparisons with a-Si:H are not very useful here), the sharpest line is probably due to electrons trapped in the conduction band tail, and the broad line is probably associated with holes trapped in the valence band tail. It is important to point out that ESR signals due to holes are not very often observed in crystalline silicon. However, if the photo-excited holes are trapped in localized, valence band tail states, which are not present in single crystals, their observation is plausible. In a-Si:H localized holes trapped in band-tail states are observed at temperatures exceeding 100 K [31]. This interpretation has the advantage that it provides a natural explanation for why no second line attributable to holes has been observed in intrinsic μc-Si:H under illumination [19,32,33]. The explanation is simply that the feature previously attributed to a single line is actually due to the sum of two.

Previous ESR studies [16,23,33] of doped μc-Si:H are generally consistent with the above explanation. The absence of any signal clearly identified with holes in valence band tail states in boron doped μc-Si:H [34] is not a surprise since the doping process in μc-Si:H is very different from that in a-Si:H. Since any localized band-tail states in μc-Si:H probably exist at interfaces and have much narrower distributions in energy than in a-Si:H, it is probable that the holes are trapped at the relatively deep acceptors in the bulk and not in the band-tail states at the interfaces. In n-type μc-Si:H the shallower donors may, in fact, contribute electrons to the band-tail states at the interfaces.

4. UNIVERSAL DECAY OF TRAPPED CHARGE CARRIERS IN a-Si:H

Using the ESR technique, we have made considerable progress on understanding the decay of optically excited carriers in a-Si:H at low temperatures and short times. The discovery in 1989 by Shklovskii et al. [35] that the simultaneous diffusion and recombination of electron-hole pairs in amorphous semiconductors is a universal property that does not depend on the densities of localized band-tail states has prompted renewed interest in the low temperature recombination processes in hydrogenated amorphous silicon (a-Si:H). At short times and low temperatures, hopping of the carriers downward in energy plays a major role in recombination, and at long times carriers become effectively trapped and recombination via tunneling is the only important process. Short times (t < 1 ms) have been probed in photoluminescence (PL) or photoconductivity (PC) experiments [36] while long times (t > 10 s) have been probed in optically excited electron spin resonance (LESR) experiments [37]. We have examined the recombination kinetics of short-lived photo excited carriers in a-Si:H at low temperatures using LESR. At temperatures below 100 K, previous measurements have shown that there is not a unique relaxation lifetime for the optically excited carriers, but rather the lifetimes vary by several orders of magnitude [37,38]. The previous LESR experiments concentrated on the long time decays where the theoretical interpretation is less complex. On shorter time scales there are

two competing processes, quantum tunneling by a single carrier to a lower energy state and recombination of an electron and a hole via tunneling [35]. At these shorter times we observe departures from the so-called universal decay [37] that occurs solely because of recombination between long-lived, band-tail carriers. In addition to testing the theoretical models [35], an examination of the recombination of charge carriers at shorter times allows the LESR data to overlap with previously published PL and PC data [36]. Finally, at shorter times and lower excitation intensities, one may perhaps find direct evidence for geminate recombination.
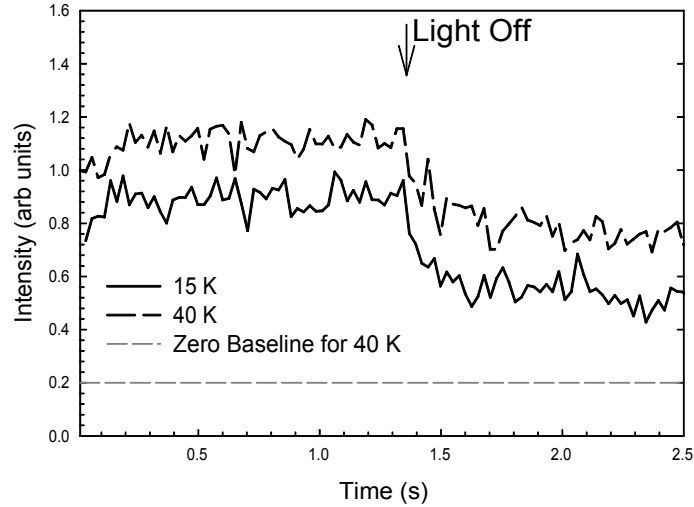
Figure 8. Short-time decay of the LESR after the light is turned off. Note that the zero for the curve at 40 K is displaced by 0.2. The arrow indicates the time at which the light was turned off.

A second general reason for performing these shorter time experiments is to connect with nuclear magnetic resonance (NMR) measurements of the dipolar relaxation times, T_{1d}, of ^{1}H in a-Si:H [39,40]. In these experiments T_{1d} has been interpreted as due to a cross-relaxation process between hydrogen nuclei and paramagnetic electrons, either silicon dangling bonds or electrons and holes trapped in band-tail states. Optical excitation at short times and low temperatures [40] produces a decrease in T_{1d} that is attributed to a specific density of trapped, band-tail electrons and holes. The present LESR experiments, which were performed on the same samples under the same conditions, provide an independent estimate of the density of paramagnetic electrons and holes that is consistent with the value inferred from the NMR measurements.

Figure 8 shows a decay curve taken at 15 K (solid line) that is obtained under circumstances identical to those used in the above-mentioned T_{1d} experiments. The data in Fig. 8 have been smoothed using a five-point averaging technique. The dashed line shows data taken at 40 K, and they are identical to the results at 15 K within experimental error.

Figure 9. Decay of LESR on (a) short and (b) long time scales. The initial LESR intensities for (a) and (b) are 2 and 1, respectively. The scales in (a) and (b) are arbitrary. The actual initial intensities were the same in both cases within experimental error.
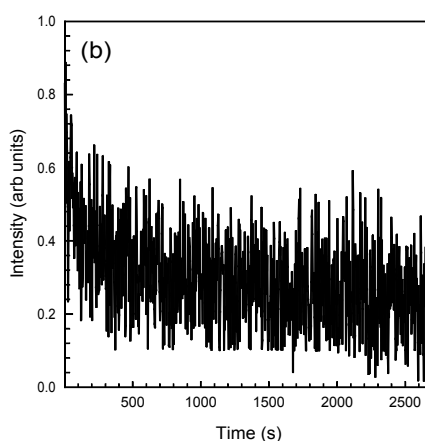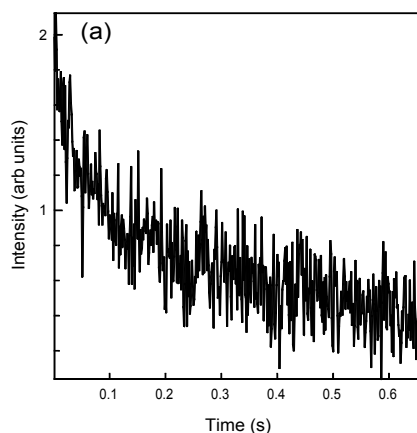
Figure 9 (a and b) shows the LESR decay curves after saturation of the LESR signal in the steady state. The zero in time is immediately after the light was turned off. These two curves represent the shortest and longest time scales employed in this study: (a), 655 ms, and (b) 2600 s. The curve that extends over 655 ms [Fig. 9(a)] involves significant signal averaging.

Figure 10 is a composite plot of the intensity of the LESR decays on a log time scale. Note that the composite curve covers six orders in magnitude in time. The intensities of the various components were scaled to essentially the same starting intensity and the raw data were smoothed as described for Fig. 8. The data indicated in gray are the previously published long time data of Yan et al. [37], which agree quite well with the present results. [The present results were taken using acquisition parameters that were kept as constant as possible to avoid systematic errors. Therefore, the signal-to-noise ratios at longer times can be greatly improved by optimizing these parameters for longer times.]
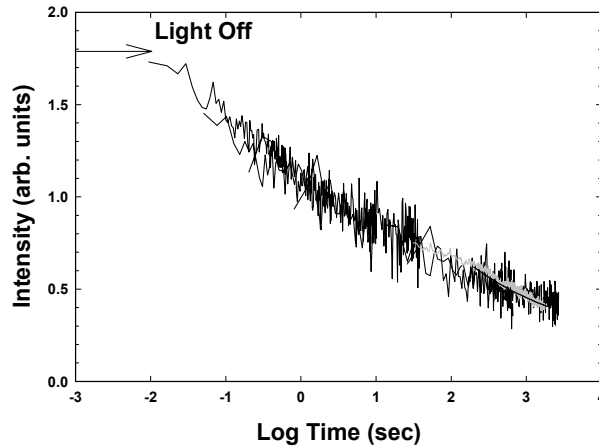
Figure 10. Decay of LESR on a log time scale. The arrow marks the initial intensity. The figure consists of several different runs on different time scales as described in the text. The gray data between about 30 and 2000 seconds are from previously published long time measurements [3].

The fact that the decays in Fig. 8 are the same at 15 and 40 K confirms the previous suggestion [37,38] that up to at least 80 K the effect of temperature can be neglected as is assumed in the models [35]. Therefore, the data taken in the previous and present studies at 40 K can be directly compared with the predictions of ref. [35], which assumed T = 0 K.

The LESR intensity with the light on (t < 1.3 s) in Fig. 8 was estimated using several methods. First, estimates were obtained by comparing the first harmonic LESR signal at 15 K and 40 K with a calibrated standard run at 15 K, 40 K and 292 K. Although very small signal-to-noise ratios and the unavoidable effects of saturation due to the applied microwave power make these estimates rough, the density is between 10^{16} and 10^{17} cm^{-3}. A comparison with the more accurate long time data taken previously [37] where the starting LESR spin densities are much more accurately known (gray data in Fig. 3) suggests that the initial density for the spectrum in Fig. 1 is between 5 x 10^{16} and 1 x 10^{17} cm^{-3}. This density decays by approximately a factor of two after 100 ms. The T_{1d} NMR experiments, which sampled the optically induced band-tail carriers approximately 100 ms after the light was turned off, yielded an order of magnitude estimate for the density of 10^{17} cm^{-3}. Given the uncertainties in the two measurements, the LESR and NMR estimates are consistent. This consistency provides a stringent test of the interpretation that T_{1d} in a-Si:H is due to cross relaxation of the protons with paramagnetic electrons and holes.

In Fig. 11 we re-plot the data of Fig. 10 as one over the cube root of the intensity as a function of ln(t). We do this because at long times the LESR intensity will become proportional to ln^{-3}t.
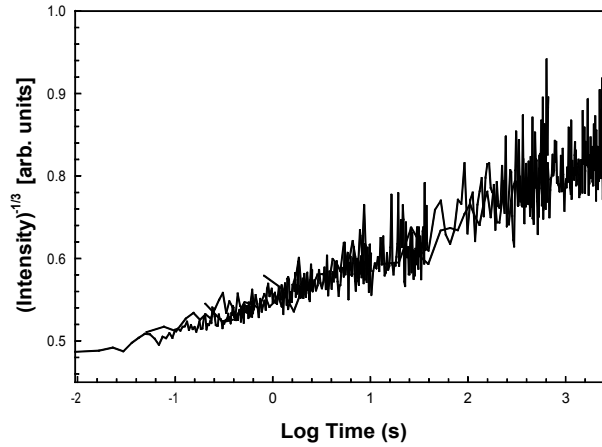
Figure 11. Inverse of the cube root of the LESR intensity as a function of the logarithm of time.

At shorter times the data of Fig. 11 show that there are clear departures from the asymptotic behavior as expressed in eq. (2). In fact, the behavior expressed in eq. (2) is never accurately achieved, even after several thousand seconds. Although the data are noisy at long times, one can see in Fig. 11 an approach to a linear relationship at long times. The shortest times in Figs. 10 and 11 approach the longest times for which the PL has been measured in a-Si:H [41]. Therefore, future measurements should allow a direct comparison between the LESR and PL measurements over the same time scale.

Modeling of the eventual recombination of optically excited electrons and holes in amorphous silicon at low temperatures (T < 40 K) involves two distinct processes, the hopping down in energy via tunneling of each individual carrier (diffusion) and recombination of electrons and holes via tunneling. At short times the hopping down processes dominate, and at long times the recombination processes dominate. On shorter time scales (t < 1 s) and at low temperatures the two processes compete: quantum tunneling by a single carrier to a lower energy state, and recombination of an electron and a hole via tunneling [35]. At finite temperature where excitations that increase the energy are possible, a third mechanism, namely variable range hopping of the charge carriers, must be considered. The optically induced electron spin resonance (LESR) signal of amorphous silicon at low temperatures has been well studied for time scales greater than about 1 s [43,43]. The photoluminescence (PL) signal, which is related to the LESR, in amorphous silicon has also been well studied for time scales less than about 1 ms [44]. We have studied the temperature dependence of the growth and decay of the LESR on short and long time scales (10^{-3} < t < 2500 s) in between the previously published photoluminescence and the LESR data. In addition, we have examined the saturated density of charge carriers as a function of temperature and excitation intensity. Eventually, these measurements will lead to a better understanding of the band tail structure of amorphous silicon as well as the kinetics of the excitation and recombination processes.

Figure 12 shows the LESR decay curves after saturation of the LESR signal in the steady state. The zero in time is immediately after the light was turned off and the colored (shaded) arrows to the left of the graph indicate the saturated densities. The red, green, yellow, blue, and black curves (top to bottom) show data taken at 40 K, 80 K, 90 K, 100 K, and 110 K, respectively. Below 40 K the data are essentially independent of temperature. The saturated densities are down by at least a factor of ten by 150 K. This general behavior can be understood in terms of variable range hopping, which becomes important above about 50 K. At higher temperatures the carriers can recombine more rapidly because of variable range hoping, and therefore the saturated densities of carriers decrease with increasing temperature for constant excitation intensity.

A comparison of the data taken at 40 K (red data) with those taken at 80 K (green data, darker middle curve) or 90 K (yellow data, lighter middle curve) shows the qualitative differences introduced by the effects of finite temperature. Initially, the carriers decay more rapidly because variable range hopping allows them to come into closer proximity with each other on short time scales. This trend continues at higher temperatures, but one must expand the time scale of Fig. 12 to see the rapid decays at temperatures above about 90 K.

At longer times the decay at elevated temperatures becomes slower than that observed over the same times at low temperatures. This result also is due to the residual effects of the variable range hopping, which allows the more shallowly trapped carriers to recombine faster leaving a smaller number of deeply trapped carriers to recombine as slowly as they do at low temperatures. Effectively, the influence of variable range hopping is to clear the band tails of carriers so that the recombination of long-lived carriers is observed at shorter times.

So far we have discussed the fact that modeling of the eventual recombination of optically excited electrons and holes in amorphous silicon at low temperatures (T < 40 K) involves two distinct processes, the hopping down in energy via tunneling of each individual carrier (diffusion) and recombination of electrons and holes via tunneling [35]. At short times the hopping down process dominates, and at long times the recombination process dominates. On intermediate time scales ($10^{-3} < t < 1$ s) and at low temperatures the two processes compete: tunneling by a single carrier to a lower energy state, and recombination of an electron and a hole via tunneling. We have also discussed the fact that at finite temperature where excitations that increase the energy are possible, a third mechanism, namely variable range hopping of the charge carriers, must be considered. We now consider measurements that extend the LESR results down to time scales approaching those probed in the PL experiments (1 ms). We also examine in more detail the temperature dependence of the decay of optically excited carriers over a wide range of times from approximately 10^{-3} s to 10^{3} s.

At finite temperature where excitations that increase the energy are possible one would expect a more rapid diffusion of carriers and therefore enhanced recombination. Unlike the low temperature behavior, this diffusion, or variable range hopping, will depend on the details of the densities of localized band-tail states. Short times (t < 1 ms) and low temperatures have been probed in photoluminescence (PL) or photoconductivity (PC) experiments [44] while long times (t /10 s) have been probed in LESR experiments [42,43,37]. At temperatures up to 100 K there is no unique relaxation lifetime for the optically excited carriers, but rather the lifetimes vary by

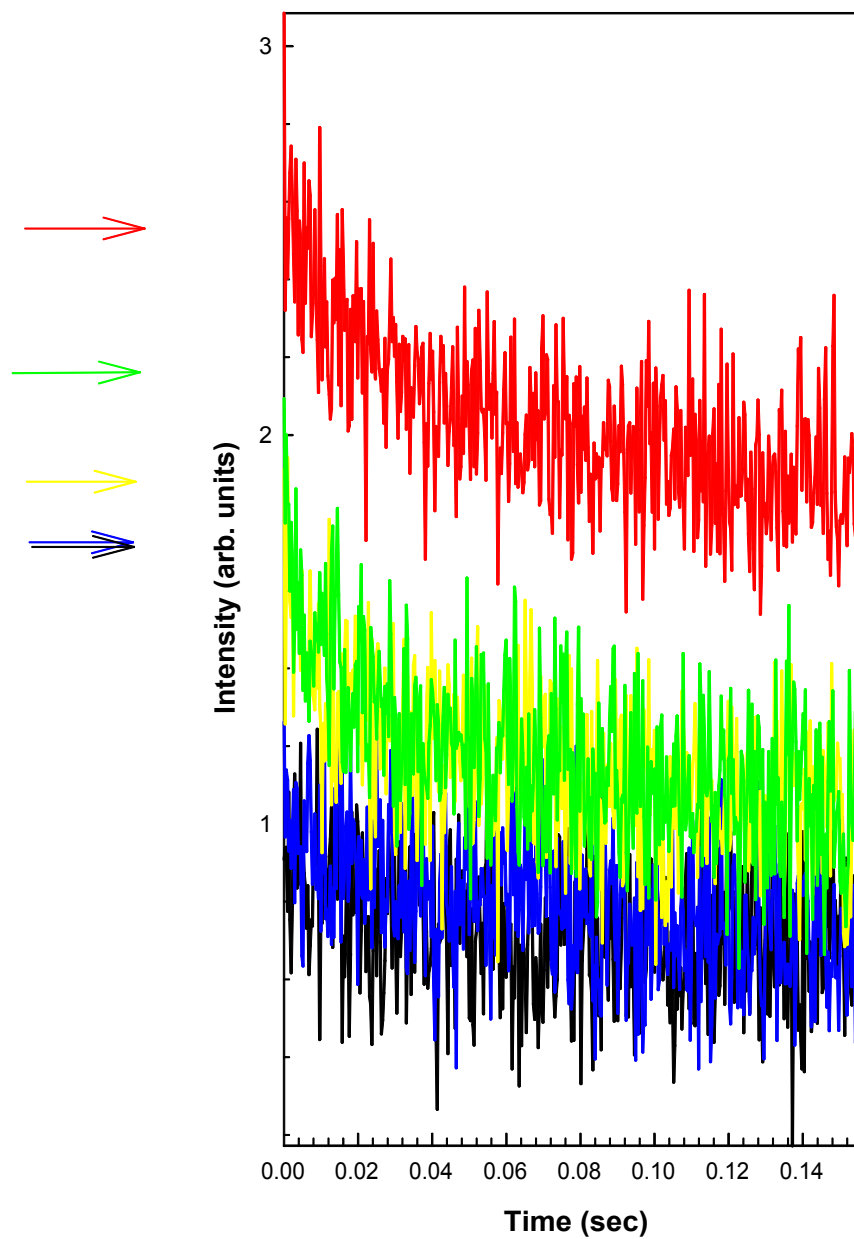**Temperature Dependent Decay of Charge Carriers**

Figure 12. Decay of LESR on short time scales as a function of temperature. The colored arrows at the left indicate the initial, saturated LESR intensities. The red, green, yellow, blue, and black curves represent data taken at 40 K, 80 K, 90 K, 100 K, and 110 K, respectively. See text for details.

many orders of magnitude [42,37]. The previous LESR experiments concentrated on low-temperature, long-time decays where the theoretical interpretation is less complex. On shorter time scales there are two competing processes, tunneling by a single carrier to a lower energy state and recombination of an electron and a hole via tunneling. Even at these shorter times the decays are "universal" in the sense that the do not depend on the densities of localized band-tail states.

Figure 13 shows the saturated, steady state spin density as a function of temperature. Although the initial light intensity remains unchanged at 1 mW/cm^2 the steady state number of spins decreases with temperature. The density decreases with increasing temperature because of the increased ability of the carriers to hop to higher energy states (variable range hopping) and therefore to recombine more readily. For this reason the number of steady state charge carriers decreases with temperature. This behavior has been known for many years.
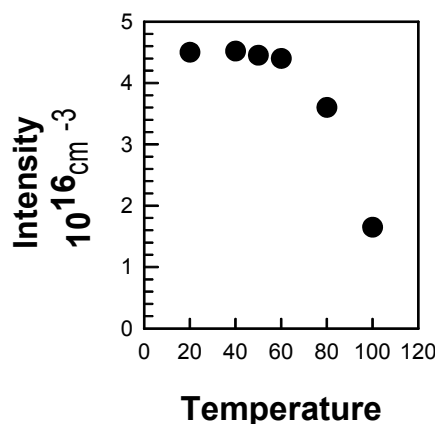
Figure 13. Temperature dependence of the saturated, steady-state LESR spin density in a-Si:H under irradiation at 632.8 nm with an intensity approximately 1 mW/cm^2.

Typical LESR decays are shown in Figure 14. As will be discussed below, the two general features that appear as temperature increases – a more rapid decay at short times and a slower decay at long times – are consistent with the expectations of the variable-range hopping process.

Figure 15 shows the decay of the charge carriers with time over a wide range of times (six decades). Although some of the details at short times are lost on the log time scale, the lower temperatures clearly exhibit a different shape than the higher temperatures. Data taken at 40 K and 50 K are not shown for clarity. The decays at 40 K and 50 K are very similar to that at 60 K. On the log time scale, the100K curve appears to be almost flat, and there is a significant drop in the intensity at times shorter than those measured.

Figure 14. The short time decay of charge carriers in a-Si:H at 20, 60, 80 and 100 K. Arrows indicate the saturated, steady-state LESR spin densities. See text for details.
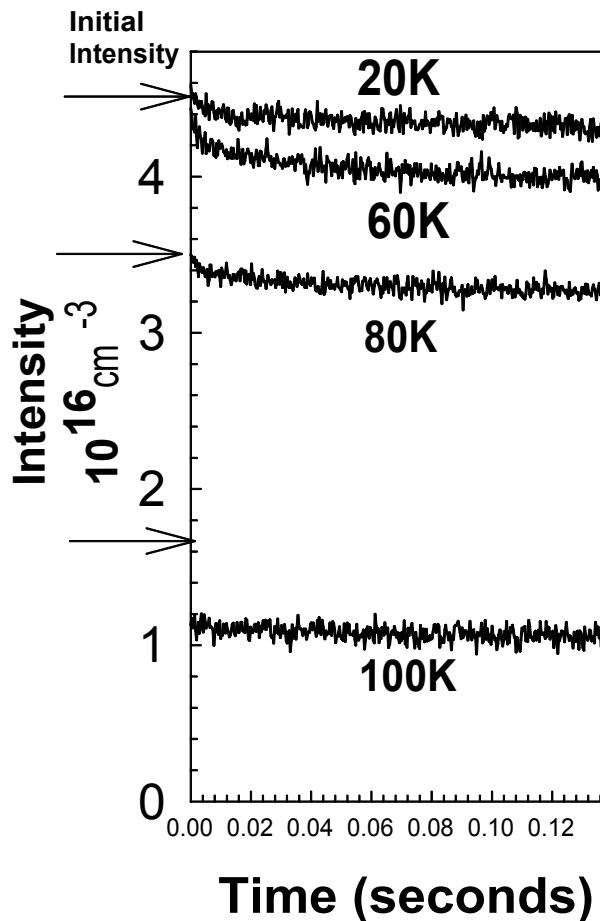
Figure 16 shows the long time decay curves of the LESR at 20 K and 100 K. The gray lines through the data are fits that will be described below. These fits start at 10 seconds using a procedure described below.

The LESR intensities with the light on (Fig. 13) were obtained by comparing the first harmonic LESR signal at all temperatures with a calibrated standard run at 292 K. Due to the standard difficulties in measuring absolute intensities in ESR, these estimates are correct to within plus or minus a factor of approximately two. The relative errors are less than the sizes of the data points. As seen in Fig. 13, the density is essentially constant up to about 60 K above which it decays rapidly with temperature.

In addition to the decrease in the saturated steady-state spin density with temperature, two qualitative features are discernable from the data in Figs. 14 and 15. As the temperature increases the short time decay becomes more rapid. This is particularly evident at 100 K where there is considerable decay at times shorter than the shortest measurement times (a few ms). This enhancement in the short time decay is consistent with the onset of variable range hopping

because the increased diffusion of the carriers will lead to an increased probability for recombination. The second qualitative feature is that with increasing temperature the decay rates actually decrease at the longer times. This behavior is also particularly evident in the 100 K data of Figs. 14 and 15. This behavior is also a consequence of variable range hopping. Although diffusion of the carriers results initially in a more rapid decay, those few carriers that remain at longer times are trapped deeply enough that temperature no longer plays a significant role.

Figure 15. The decay of charge carriers in a-Si:H at 20, 60, 80 and 100 K on a log time scale. Arrows indicate the saturated, steady-state LESR spin densities. See text for details.
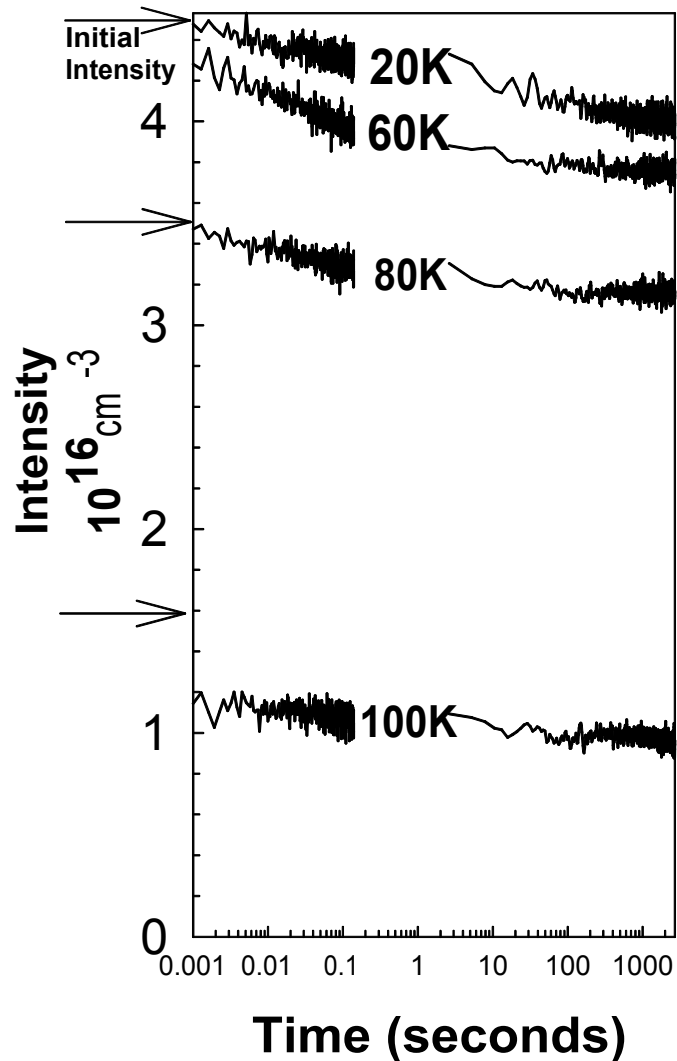
Figure 16. Decay of the LESR in a-Si:H as a function of time at low and high temperatures. The gray lines through the data are "zero" temperature fits as described in the text. The inset shows the shorter time data on an expanded scale.
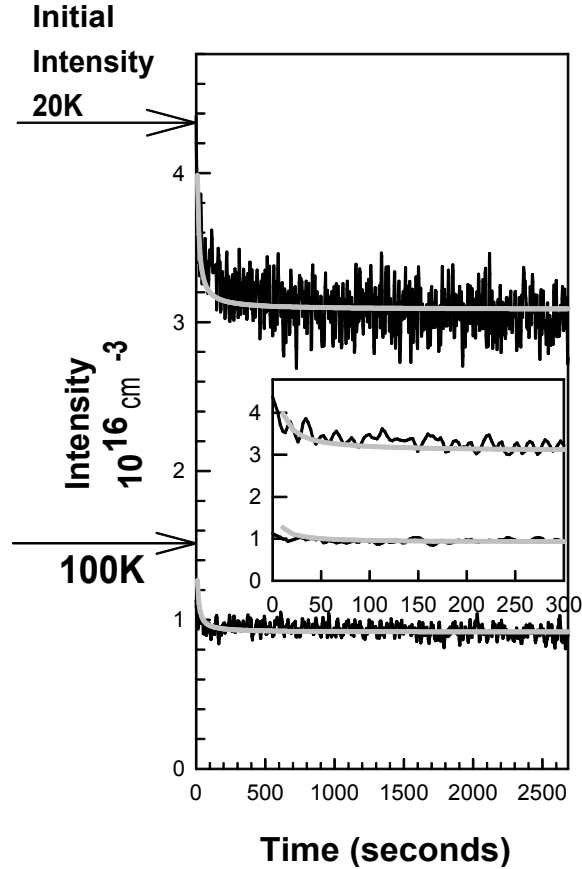
At "zero" temperature, where only hopping downward in energy is possible, and at the longest decay times the LESR intensities should converge on a common value, $n(t)$, which is independent of the initial intensity (independent of the generation rate). This asymptotic behavior, which is logarithmic in t, and therefore highly non-exponential, is "universal" in the sense that it depends neither on the original excitation intensity nor on the shapes of the valence and conduction band tails of localized electronic states. Due to the difficulty in estimating the time at which downward hopping is no longer important, the decay curves are usually fit to the appropriate functional form after a specific time, in our case 10 s. This fitting amounts to scaling the data for one of the decay curves to eliminate the uncertainties in the absolute value of the spin density. After fitting one decay curve, all others at different excitation intensities are obtained by using the initial spin densities, but with no further adjustable parameters.

In Fig. 16 this procedure has been applied to two curves, one at 20 K and one at 100 K. Clearly, the zero temperature approximation does not apply to 100 K, but the fit using only the steady-state value of the spin density is remarkable. This agreement confirms the comment made above that the only carriers remaining at long times are those trapped deeply enough such that temperature no longer plays a role. At the longest times, the only effect of finite temperature is to reduce the steady-state spin density at constant excitation intensity.

Although the simultaneous diffusion and recombination of optically excited carriers at low temperatures is a universal property of amorphous semiconductors, the shapes of the decay

curves at elevated temperatures do depend on the densities of localized band tail states. Therefore, at higher temperatures one expects the decay curves to be different for different materials.

In summary, at an excitation intensity of approximately 1 mW/cm^2 the decay of the LESR in a-Si:H exhibits three qualitative features with increasing temperature. First, the saturated, steady-state densities decrease rapidly above approximately 60 K. Second, the long time decay (at times greater than a few seconds) at elevated temperatures can be fit using a low temperature approximation presumably because the carriers that remain are trapped deeply enough that temperature is no longer a factor in recombination. Third, the short time decay (at times less than a second) increases progressively with increasing temperature presumably because of the effects of variable range hopping.

5. THE STAEBLER-WRONSKI EFFECT IN a-Ge:H

For over 25 years the Staebler-Wronski (SW) effect has persisted as the fundamental metastability in hydrogenated amorphous silicon (a-Si:H). This effect has also been observed in some hydrogenated amorphous silicon-germanium alloys with low concentrations of germanium. The SW effect was originally observed [4] as an optically induced, metastable decrease in both the dark and photoconductivities, but soon afterward this effect was tied to a concomitant increase in the electron spin resonance signal [45] commonly attributed to silicon dangling bonds. Over the years there has been some speculation concerning the existence of the SW effect in hydrogenated amorphous germanium (a-Ge:H) but to date no positive results have been reported. In 1991 Santos et al. [46] observed a decrease in the dark conductivity and photoconductivity in a-Ge:H, but the effect annealed at room temperature in the dark, which was also confirmed by Bauer and Eberhardt in 1993 [47]. Several authors [48,49,50] have suggested that below a specific optical gap energy, which is greater than the optical gap energy of a-Ge:H, there is insufficient recombination energy to lead to the creation of a metastable defect.

Previous studies have shown that both a-Si:H [37] and a-Ge:H [51] exhibit a universal decay of the LESR at low temperatures. Here we discuss an optically induced increase in the electron spin resonance (ESR) spin density at room temperature that can be partially annealed (approximately 30 % of the increase remains) after one hour of annealing at 170 C in a nitrogen environment. Even in the absence of optical excitation, annealing above approximately 165 C produces a small, but stable, increase in the dark spin density, presumably due to hydrogen evolution from the sample. As in a-Si:H, some of the changes are reversible (SW effect), but unlike a-Si:H the samples cannot be recycled more than a few times before the irreversible increases dominate. In comparison with the well-studied behavior in a-Si:H, a more detailed study of the kinetics of the SW effect in a-Ge:H will be important in testing possible microscopic models

Figure 17 shows the initial ESR derivative spectrum of a-Ge:H, the change in the spectrum after 10 hours of irradiation at 2 W/cm^2, and the spectrum after annealing at 170 C for one hour. After two hours of irradiation the increase in the spin density is approximately 50 % of the initial dark spin density. After ten hours irradiation, the increase is approximately 100 %. However after the annealing approximately 70% of the induced defects remain in the sample.

These are irreversible defects that do not anneal out at elevated temperatures even after longer annealing times approaching several hours. The narrow signal near 3390 gauss in Fig. 17 is due to e´ centers, which presumably occur at the a-Ge:H/SiO$_2$ interface. [The e´ center is an electron trapped in an sp^3 orbital at a silicon atom, which is bonded to three oxygen atoms.] The irradiation also produces a decrease in the e´ center, which is partially reversible on annealing. The mechanism producing the changes in the e´ center is unknown but may be due to hydrogen motion at the interface.

Figure 17. Derivative of the ESR absorption signals in a-Ge:H at 40 K. The solid, dotted and dashed lines are the initial dark signal, the signal after ten hours of irradiation at 300 K with 1 W/cm^2 of 1.17 eV light, and the signal after subsequent annealing at 171 C for one hour. All traces were run at 40 K to improve the signal-to-noise ratios.
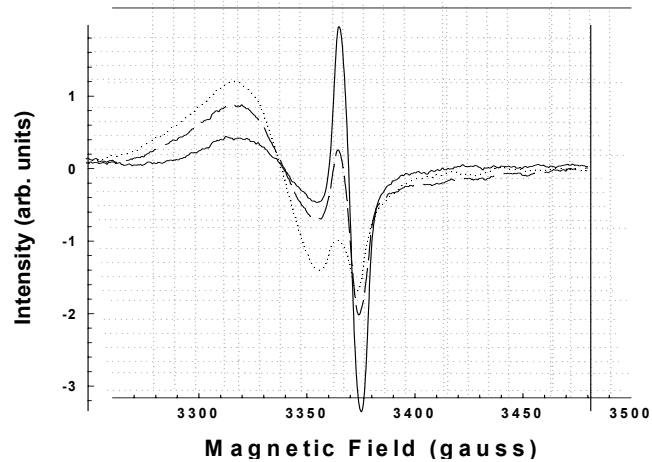
Figure 18 shows the growth of the total ESR signal in the stack of a-Ge:H films under irradiation with 0.5 and 1 W/cm^2. Both growth curves depend on time as $t^{1/3}$, which is similar to the kinetics observed in a-Si:H [52] and is representative of a broad distribution in the time constants. However, the data for a-Ge:H in Fig. 18 include all defects - the initial dark spin density, the optically induced reversible (SW effect) component, and the optically induced irreversible component. Figure 19 shows the growth curves with the initial dark spin densities subtracted. In this case, the growth appears to depart from a $t^{1/3}$ dependence, especially at short times. The heating of the sample due to the laser at the highest intensity will affect the details of the kinetics but not the overall general features. The times indicated in Figs. 18 and 19 are those that each orientation of the sample received. Because four perpendicular orientations were employed, the total irradiation times for all orientations are greater by a factor of four.

The maximum irradiation time employed at an intensity of 0.5 W/cm^2 is 30 hours, and the optically induced ESR intensity appears to saturate after approximately 20 hours. At 1 W/cm^2 the maximum irradiation time is 26 hours, and saturation occurs after approximately 15 hours. At 2 W/cm^2 the maximum irradiation time is 16 hours, and saturation occurs after approximately 10 hours.

Figure 18. Growth of the total (dark and light induced) ESR absorption signals in a-Ge:H after irradiation with 0.5 W/cm^2 of 1.17 eV light (solid circles) and 2.0 W/cm^2 of 1.17eV light (solid squares). All measurements were taken at 40 K. The dotted and solid lines are power law fits to the data with an exponent of 1/3 (t$^{1/3}$).
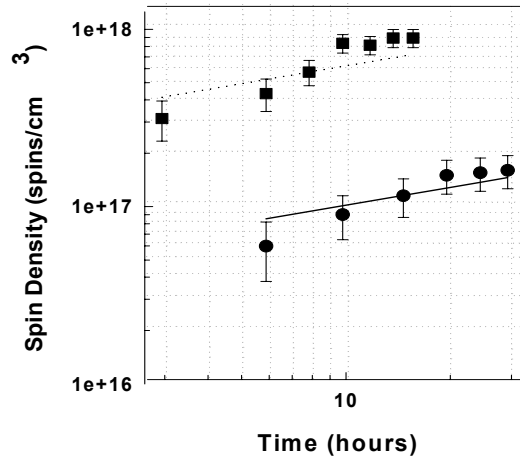
The solid curves in Fig. 19 represent exponential rises to saturation indicative of unique time constants. The dotted lines are stretched exponential rises to saturation with a stretched exponential exponent of α = 0.5. This value of α approximates the t$^{1/3}$ dependence as shown in Fig. 18 when the growth curve is not near saturation [53]. Although the initial dark spin density is subtracted from all the data points in Fig. 19, these data do not represent the SW defects because there exists an optically induced irreversible component that depends strongly on the intensity of the exciting light. At an excitation intensity of 1 W/cm^2 we have an estimate of the irreversible component at two irradiation times after which the sample was annealed, 10 hours and 26 hours. From these two data points, we estimate that the irreversible spin density appears to have essentially the same time dependence as the reversible spin density. If this is indeed the case, then subtracting the irreversible spin density from the data points in Fig. 19 will merely shift the graph downward on the log-log plot but will not change the general shape. Therefore, we conclude that the curves shown in Fig. 19 are reasonable representations of the growth of the SW defects in a-Ge:H, although the absolute spin densities are clearly not correct.

Figure 19. Growth of LESR signals in a-Ge:H after irradiation with 1.17 eV light of intensity 0.5 W/cm^2 (solid circles), 1.0 W/cm^2 (solid triangles), and 2.0 W/cm^2 (solid squares). The solid and dotted lines are fits to the data assuming an exponential rise to saturation and a stretched exponential rise, respectively.

26
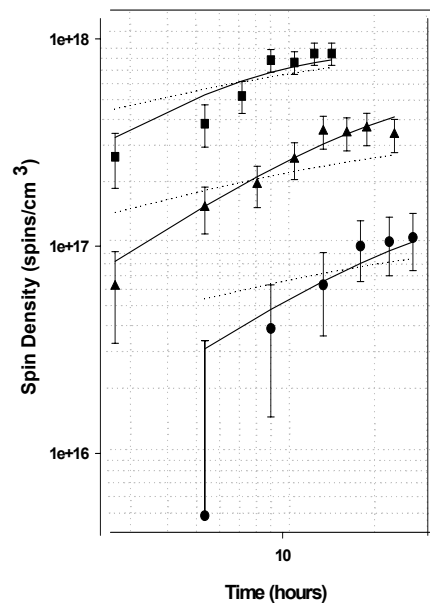
Using the saturated spin densities at the maximum times shown in Fig. 19, after which we anneal the samples, we can estimate the fraction of defects that is irreversible at these times. This fraction depends super linearly on the generation rate, G, roughly as G^2. This power dependence indicates a two-photon process. The reversible SW defects, on the other hand, are well fit to a $G^{2/3}$ dependence, just as occurs in a-Si:H. Therefore to maximize the influence of the irreversible defects one should perform the experiments as the lowest excitation intensities possible.

It is interesting to note that there is also a small irreversible component to a-Si:H after many cycles of light irradiation and annealing, but this effect has not been studied in detail [54,55]. It is quite probable that this irreversible component is a two-photon process too. In a-Ge:H this irreversible component is enhanced to such an extent that multiple cycling of samples between irradiation and annealing is very difficult. The irreversible defect density after 16 hours of irradiation at 2 W/cm^2 is more than 70% of the total optically induced defect density in the sample as measured by ESR. There is also an irreversible component due to the annealing itself, which gets larger at higher annealing temperatures. Fortunately, at the annealing temperatures employed in this study, this thermally induced component is very small compared to the light induced defect densities.

The range of practically accessible annealing temperatures in a-Ge:H appears to be much narrower than in a-Si:H. We were able to observe annealing of the SW defects between 150 and 170 C. Below 150 C the annealing times were too long to obtain reliable data and above 170 C the annealing itself produced an increase in the dark spin density that was large enough to complicate the interpretation. The annealing is probably thermally activated as it is in a-Si:H, but the primary activation energy is difficult to quantify at this time. The value is less than 1 eV and the distribution of activation energies is probably narrower than in a-Si:H. This result, coupled with the growth curves, which can be adequately fit by an exponential rise to saturation, suggests that the time constants and activation energies may exhibit narrower distributions in a-Ge:H than they do in a-Si:H.

The similarities in the kinetics for producing and annealing the dangling-bond ESR signals between a-Ge:H and a-Si:H provide strong evidence that we have observed the SW effect in a-Ge:H. However, it is the differences between these two materials that will be important in testing the various models proposed [10,52] to explain the SW effect.

We have observed the Staebler-Wronski effect in a-Ge:H by measuring a reversible increase in the ESR after optical excitation at 1.17 eV. In general, the kinetics is similar to a-Si:H, but there may be a narrower distribution of activation energies and time constants in a-Ge:H. The kinetics of the SW effect is difficult to study in detail due to the large percentage of irreversible defects, even at the lowest practical excitation intensities.

6. COMPARISON OF DEFECTS IN a-Si:H DEVICES AND FILMS

Despite over twenty-five years of scientific studies on light induced defects in hydrogenated amorphous silicon (a-Si:H) materials and solar cells there are still unanswered questions regarding their nature. It was found early on that light induced degradation created

dangling bonds. These defect states, and in particular that of the neutral dangling bond (D^0) which can be identified and its densities measured with electron spin resonance (ESR), have received the most attention. There are, however, copious results reported on a-Si:H thin films and solar cells, which clearly point to the presence of multiple light induced defects in a-Si:H. These results include a disproportion between light-induced changes in the defect densities as determined by optical absorption and those by ESR [56], the absence of consistent correlations between the changes in electron mobility-lifetime ($\mu\tau$) products and those in optical absorption below the band gap [$\alpha(E)$] [57,58,59], and isochronal annealing differences between the recoveries of $\mu\tau$ and $\alpha(1.25eV)$ [60,61]. The presence of "fast" and "slow" defect states has been well established by the studies on the recoveries of the fill factors after degradation with high intensity illumination [62,63]. These studies also showed that those states created faster also anneal out faster. The presence of such defect states is also reflected in the degradation kinetics of cells and films under 1 sun illumination where the initial and subsequent regimes exhibit distinctly different dependences on temperature [64]. There is also evidence in the results on optical absorption below the band gap for the presence of multiple light induced defects indicated by their changes not only in magnitude but also in their spectra [59]. Recently two distinctly different light induced defect states around and below the middle of the optical gap were identified from the comparison of changes in optical absorption spectra obtained for a-Si:H films with large differences in their microstructure [65,66]. This differentiation was obtained by analyzing the spectra not just in terms of a single defect state, as is generally done, but by taking into account the presence of multiple defect states. To further characterize these light induced gap states a study was undertaken on hydrogen-diluted a-Si:H that exhibits "superior" stability and reaches a degraded steady state under 1 sun illumination in < 100 hours.

We describe preliminary comparisons between the light induced changes in electron mobility lifetime ($\mu\tau$) products, the electron occupied states obtained from optical absorption measurements below the gap using dual beam photoconductivity, and the densities of D^0 states measured with electron spin resonance (ESR). Our ESR measurements on light soaked and annealed samples of a-Si:H, in collaboration with the group at Penn State University, have shown that in the light soaked sample there exists a dependence on light soaking time that is consistent with the absorption peaks measured by dual beam photoconductivity at both 0.9 and 1.1 eV.

The a-Si:H materials with a bandgap of ~1.8eV, were deposited by the group at Penn State University using a hydrogen-to-silane dilution ratio of 10 by PECVD [67]. The 0.8μm films were deposited onto n+ contacts in order to establish Ohmic behavior in photocurrents over a wide voltage range even in the annealed state. A reproducible annealed state was obtained after 4 hours at 170˚C. Photoconductivity and sub-gap absorption (measured by deal beam photoconductivity) measurements were performed at Penn State University. The dual beam photoconductivity system allowed reliable measurements of the absorption coefficient up to 0.7eV from the conduction band. The ESR experiments were conducted at the University of Utah with a Bruker Instruments ESR spectrometer with samples deposited on quartz substrates utilizing the first harmonic detection technique [38]. The measurements were carried out several days after light soaking. However, insight was obtained because no evidence for long term relaxation in ESR spin density has been observed at room temperature [68].
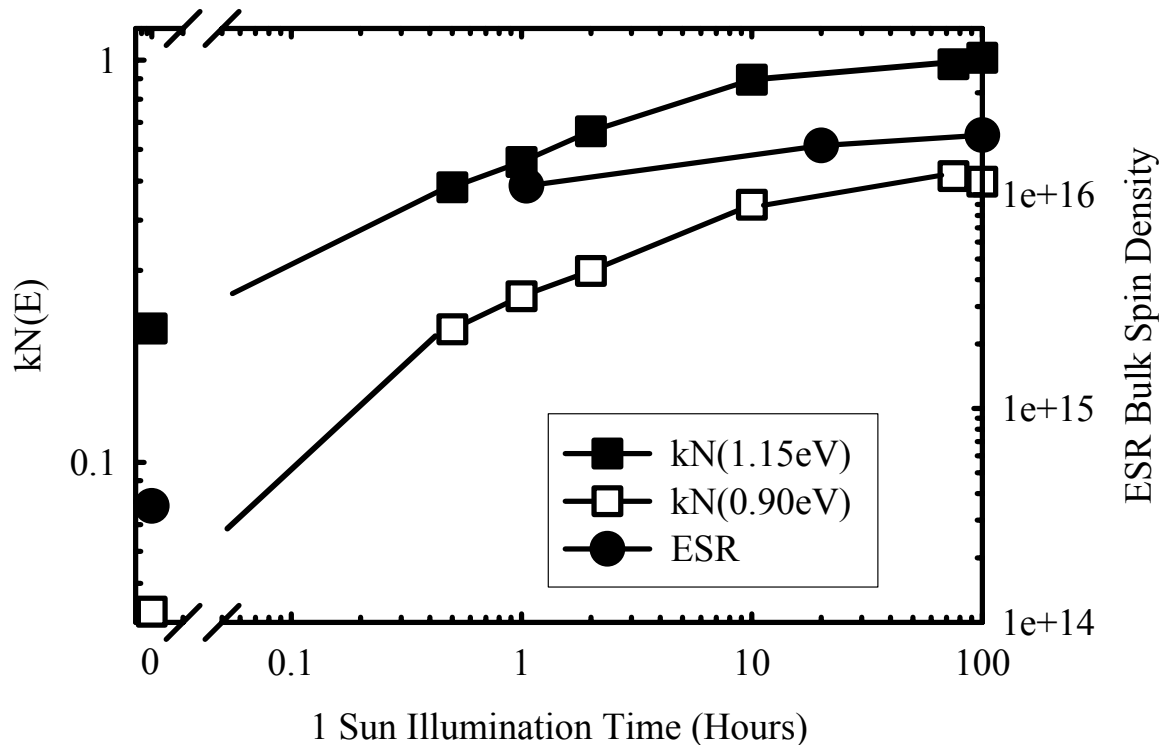
Figure 20. kN(E) at 0.9eV and 1.15eV as a function of 1 sun illumination time (left axis) and ESR bulk spin density (right axis) as a function of 1 sun illumination time.

In order to differentiate between the evolution of the states centered around 0.9eV and 1.15eV, the absorption coefficients measured by dual beam photoconductivity {kN(E) values, which for the purposes of this report we take as a measure of the optical absorption [59,65,66]} at these energies are plotted in Fig. 20 as a function of 1 sun illumination time (left axis). Also, on the right axis the bulk spin densities measured by ESR are shown for 1, 10, and 100 hour illumination times. Also shown in the figure are the values in the annealed state. The key features of the evolution of the optical absorption for both these energies are the very large increase from the annealed values in the first hour of degradation and a much slower subsequent evolution to a nearly saturated state. These features are also reflected in the ESR results. However, the similarity among the evolutions of the three results precludes at this time any conclusions as to which states can be directly related with D^0. The preliminary results on the kN(E) spectra, nevertheless, are consistent with fast and slow components to the creation of the optical absorption for both defect peaks (0.9 and 1.1 eV).

The evolution of light induced gap states centered around the middle of the optical gap and around 1.15eV from the conduction band has been characterized. The large increases in the

kN(E) spectra in the first hour of degradation are found for both the gap states and the ESR with subsequently much slower changes that approach a saturated density of states. The similarity of the kinetics in all three cases precludes any determination of which states correspond to D^0. From these preliminary results it has not been possible to draw reliable conclusions about either the actual densities or the nature of these states.

7. GROWTH AND ANNEALING OF DEFECTS IN TRITIATED a-Si:H

The appearance of optically or electrically induced defects in hydrogenated amorphous silicon (a-Si:H), especially those that contribute to the Staebler-Wronski (SW) effect, has been the topic of numerous studies [4,69], yet the mechanism of defect creation and annealing is far from clarified. We have investigated the intrinsic growth of defects in tritiated hydrogenated amorphous silicon (a-Si:H,T) as an alternative approach to inducing defects optically. Tritium decays to He^3, emitting a beta particle (average energy of 5.7 keV) and an antineutrino. This reaction has a half-life of 12.5 years; therefore, in these tritium-doped samples each beta decay can, in principle, create a defect by converting a bonded tritium to interstitial helium, leaving behind a silicon dangling bond.

We have tracked these defects through electron spin resonance (ESR) and photothermal deflection spectroscopy (PDS).   Like the optically induced defects, the defects created by tritium decay also anneal out at approximately 150 C, confirming the earlier findings from luminescence [70]. However, if each tritium decay produces a silicon dangling bond, then the observed increase in defect density is several orders of magnitude smaller than one would expect for samples that contain approximately 6 at. % of tritium. After one year, the decay of tritium to helium would be expected to yield defect densities of $\sim 10^{20} cm^{-3}$ without saturation, but the increases observed by ESR or PDS are much smaller. There might be, of course, an additional effect due to the beta particles passing through the lattice, but such an effect could only increase the number of defects beyond the tritium decay limit.

At room temperature the defect densities reach saturated values of about $10^{18} cm^{-3}$ within 1 to 4 months. At higher temperatures the saturated densities decrease rapidly.   Therefore, a very efficient annealing process must exist in the tritiated samples.

The a-Si:H,T samples were first measured after 7 years of uninterrupted tritium decay at 300 K. These initial spin densities in all three samples were orders of magnitude lower than would be expected if each tritium decay produced a silicon dangling bond. Figure 21a and b shows the annealing behavior of the initial spin densities of two samples of a-Si:H,T. Figure 21a shows the annealing behavior of the sample deposited at 250 C, and Fig. 21b shows the annealing of the sample deposited at 225 C.   It is interesting to note that the defects anneal in a manner that is very similar to the annealing of light induced defects in the non-tritiated a-Si:H. The initial (saturated) spin densities of the 250 C and the 225 C samples were 1.6 x 10^{18} spins/cm^3 and 1.2 x 10^{17} spins/cm^3, respectively. The final (annealed) spin densities after annealing of the 250 C and the 225 C samples were 7 x 10^{17} spins/cm^3 and 2.7 x 10^{16} spins/cm^3, respectively. The annealed spin densities did not decrease further with increased annealing time at 150 C.
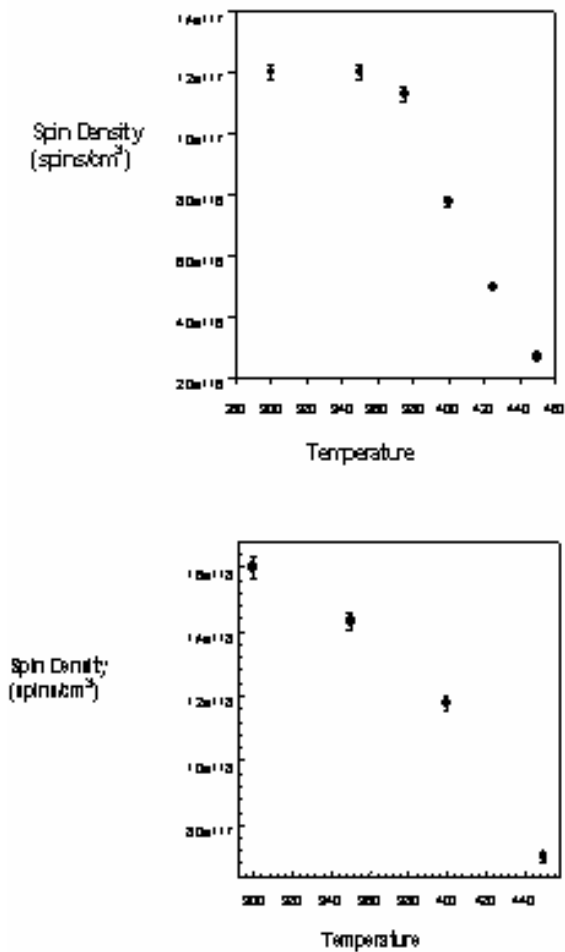
Figure 21. (a) Annealing behavior in a-Si:H,T made at a substrate temperature of 150 C. (b) Annealing behavior in a-Si:H,T made at a substrate temperature of 250 C.

The annealing can be understood, in principle. First, it is well known that the light-induced defects anneal out at temperatures below about 200 C. In addition, the number of defects in films from which H has evolved is much less than the number of H atoms that have left the films. If hydrogen is mediating the annealing of light-induced defects, which seems quite certain, then it must come from a reservoir such that the new dangling bonds created by evolving H will be healed by some structural rearrangements. Even if the sample is annealed at temperatures low enough such that no hydrogen leaves the sample, optically induced defects can still be annealed. In one specific model, H comes from a metastable complex containing paired hydrogen atoms (as suggested by Branz) [10].

Figure 22 (a, b and c) shows the growth of defects as a function of time after annealing as measured by ESR. The log of the spin density is plotted against the log of the time. Figure 22a

shows a-Si:H,T deposited at 150 C; Figure 22b shows a-Si:H,T deposited at 225 C; and Figure 22c shows a-Si:H,T deposited at 250 C. The initial spin density was measured immediately after one hour of annealing at 150 C. We measured the spin density as a function of waiting time at room temperature (circles). The spin densities increase rapidly at first and then saturate at the long-time (7-year) values. The final data point in each graph is the initial spin density of the sample before the annealing process, seven years after deposition. The saturated spin densities are all much smaller than those one would predict if each tritium decay produced a neutral silicon dangling bond. The small densities of defects were first suspected to be the result of the production of charged dangling bonds in the sample, which are not detectable by ESR. However, the growth of defects as measured by PDS (triangles) is in one-to-one agreement with the ESR proving that most of the dangling bonds are uncharged.

ESR only measures the uncharged dangling bond, and therefore a relatively small defect density might be the result of charged dangling bonds in the samples. However, PDS measures both charged and uncharged defects. The triangles in Fig. 22a, b and c represent the growth of the absorption coefficient as measured by PDS at 1 eV. The growth of the absorption coefficient and the ESR follow the same trends within the noise. The magnitude of the PDS absorption coefficient when scaled in the standard fashion [71] agrees quantitatively with the ESR signal, implying that most of the dangling bond defects in the a-Si:H,T are uncharged.
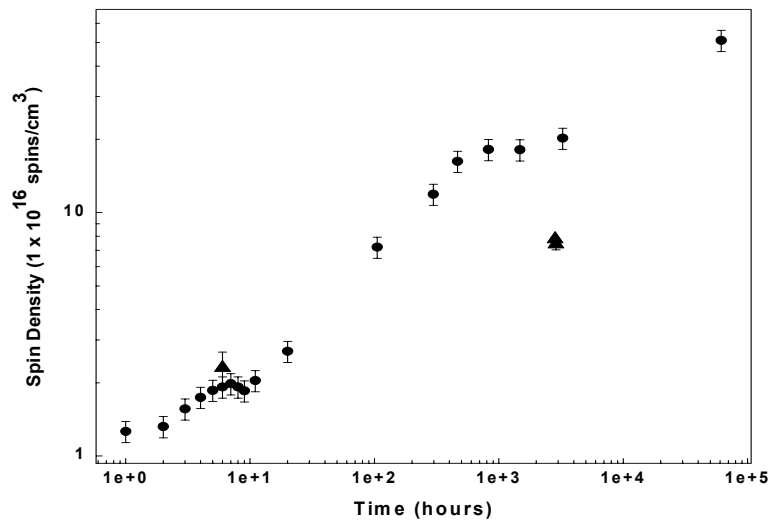

Figure 22a. The circles represent the growth of the spin densities as measured by ESR, and the triangles represent the growth of the PDS signal at 1 eV for the sample made at 150 C (log-log plot).

Figure 22b. The circles represent the growth of the spin densities as measured by ESR, and the triangles represent the growth of the PDS signal at 1 eV for the samples made at a 225 C (log-log plot).

Figure 22c. The circles represent the growth of the spin densities as measured by ESR, and the triangles represent the growth of the PDS signal at 1 eV for the sample grown at 250 C (log-log plot).

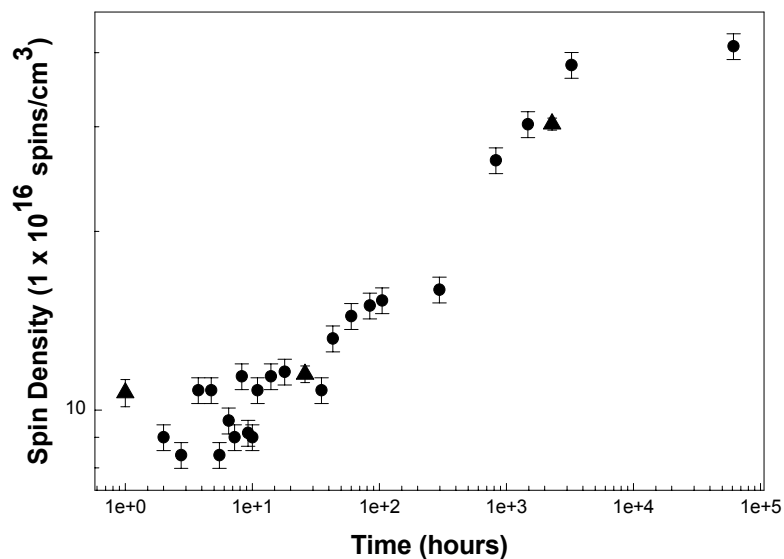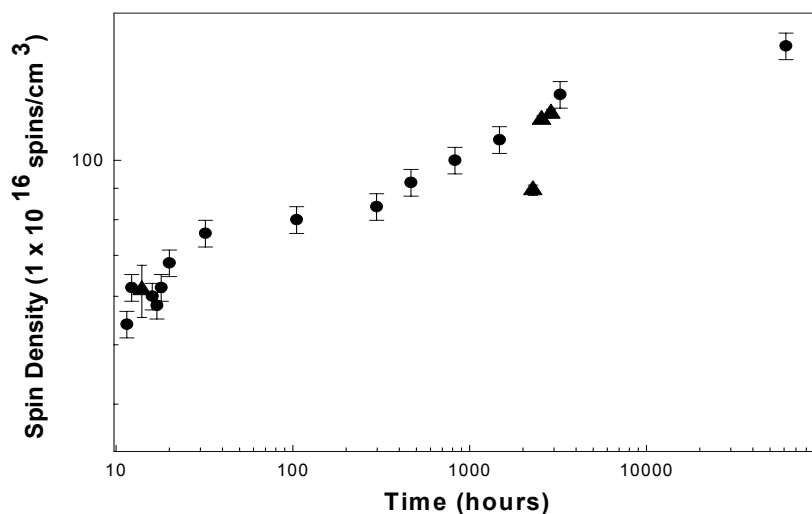These growth curves from the ESR and PDS experiments seem to be governed by some very efficient defect annealing process. Some annealing process at room temperature counterbalances the rapid creation of spins, such that the spin density saturates at much lower

33

values than predicted by tritium decay. In contrast to the light- or electron-beam-induced defects, in these tritium experiments we know exactly the rate at which defects are initially created.

8. SUMMARY

We have studied the morphology of microcrystalline films using AFM and the defects using ESR. We have completed our studies of the stability of cells made using silicon-sulfur alloys for the intrinsic layer. Also, we have compared defects measured by ESR with defects measured by CPM in PV devices made at Pennsylvania State University. These comparisons confirm the presence of two distinct defects involved in the Staebler-Wronski effect but have not yet identified which defect measured by CPM corresponds to the one measured by ESR. Second harmonic detection of LESR has been employed to measure the universal decays of band-tail electrons and holes in a-Si:H and a-Ge:H. The Staebler-Wronski effect has been observed for the first time in a-Ge:H using ESR. Investigations of the optically induced production of silicon dangling bonds in a-Si:H at low temperatures have been completed. In addition, the role of a metastable paired hydrogen defect (H doublet) has been investigated using NMR in samples of a-Si:H grown by PECVD, with and without hydrogen dilution. This hydrogen doublet is probably the defect responsible for stabilizing the silicon dangling bonds that are produced in the Staebler-Wronski effect. Initial theoretical calculations are consistent with the site being a specific type of dihydride bonding (SiH_2) site. In addition, we have initiated a novel way of looking at defect generation in a-Si:H, namely the production of silicon dangling bonds by decay of tritium (^3H), which is bonded to silicon. The tritium decays to helium, which does not bond to Si. Finally, PL from Er^{3+} in partially crystalline a-Si:H has been measured. A review of some of the earlier work performed under this sub-contract has also been published.

The most significant results of the three phases of the sub-contract are (1) the discovery of a paired hydrogen site in light-soaked a-Si:H that is probably the stabilization mechanism for the silicon dangling bonds created in the Staebler-Wronski effect, (2) the confirmation of universal kinetics for the decay of optically excited electrons and holes in a-Si:H and a-Ge:H at low temperatures, (3) the first detection of the Staebler-Wronski effect in a-Ge:H, (4) the use of a novel decay of tritium in a-Si:H to probe the production of silicon dangling-bond defects, and (5) the comparison of ESR and CPM measurements of defects in a-Si:H material used in cells.

9. REFERENCES

1. C. G. Van de Walle, Phys. Rev. B **49**, 4579 (1994).
2. K. J. Chang and D. J. Chadi, Phys. Rev. Lett. **62**, 937 (1989).
3. S. B. Zhang and W. B. Jackson, Phys. Rev. B **43**, 12142 (1991).
4. D. Staebler and C. R. Wronski, Appl. Phys. Lett. **31**, 292 (1977).
5. T. Su, S. Chen, P. C. Taylor, R. S. Crandall, and A. H. Mahan, Phys. Rev. B **62**, 12849 (2000).
6. D. E. Carlson, K. Rajan, and D. Bradley in *Proc. 26th Photovoltaic Specialists Conf. (IEEE, New York, 1997), p. 595.*
7. T. Su, P. C. Taylor, D. E. Carlson, and G. Ganguly, Phys. Rev. Lett. **89**, 15502 (2002).
8. T. Su, P. C. Taylor, D. E. Carlson, and G. Ganguly, J. Non-Cryst. Solids,   (2004).
9. S. Zafar and E. A. Schiff, Phys. Rev. B **59**, 5498 (1999).
10. H. Branz, Phys. Rev. B**59** (1999) 5498.
11. D. J. Chadi, Appl. Phys. Lett. **83**, 3710 (2003).
12. C. G. Van de Walle and B. Tuttle, MRS Symp. Proc. **557**, 275 (1999).
13. D. E. Carlson, Appl. Phys. A **41**, 305 (1986).
14. D. E. Carlson, K. Rajan, and D. Bradley, in Proc. 26th IEEE Photovoltaic Specialists Conf., IEEE, New York, 1997, p. 595.
15. F. Finger, C. Malten, P. Hapke, R. Carius, R. Flückiger, and H. Wagner, Phil. Mag. Lett. **70** (4), 247 (1994).
16. C. Malten, F. Finger, P. Hapke, T. Kulessa, C. Walker, R. Carius, R. Flückiger, and H. Wagner, Mater. Res. Soc. Symp. Proc. 358, 757 (1995).
17. J. Muller, F. Finger, C. Malten, and H. Wagner, J. of Non-Crystalline Sol. **227-230**, 1026 (1998).18118
18. M. Kondo, S. Yamasaki, and A. Matsuda, J. Non-Crystalline Sol. **266-269**, 544 (2000).
19. M. Kondo, T. Nishimiaya, K. Saito, and A. Matsuda, J. Non-Crystalline Sol. **227-230**, 1031 (1998).
20. W. Fuhs, P. Kanschat, and K. Lips, J. Vac. Sci. Technol. B **18**, 1792 (2000).
21. P. Kanschat, K. Lips, and W. Fuhs, J. Non-Crystalline Sol. **266-269**, 524 (2000).
22. See, for example, P. C. Taylor in <u>Materials Issues in Applications of Amorphous Silicon Technology</u>, Vol. 49, D. Adler, A. Madan and M.J. Thompson, eds. (Materials Research Society, Pittsburgh, 1985), p. 61.
23. F. Finger, J. Müller, C. Malten, R. Carius, and H. Wagner, J. Non-Crystalline Sol. **266-269**, 511 (2000).
24. T. Umeda, S. Yamasaki, J. Isoya, and K. Tanaka, Phys. Rev. B **59**, 4849 (1999).
25. M. Sprenger, S. H. Muller, E. G. Sieverts, and C. A. J. Ammerlaan, Phys. Rev. B **35**, 1566 (1987).
26. G. D. Watkins and J. W. Corbett, Phys. Rev. **138**, A543 (1965).
27. Y. H. Lee and J. W. Corbett, Phys. Rev. B, **8**, 2810 (1973).
28 V. C. Venezia *et al*., Appl. Phys. Lett. **79**, 1273 (2001).
29. S. Chakravarthi and S. T. Dunham, J. Appl. Phys. **89**, 4758 (2001).
30. J. C. Knights, D. K. Biegelsen, and I. Solomon, Sol. State Commun. **22**, 133 (1977).
31. R. A. Street and D. K. Biegelsen, and J. C. Knights, Phys. Rev. B **24**, 969 (1981).
32. F. Finger, J. Müller, C. Malten, and H. Wagner, Phil Mag B **77**, 805 (1998).

33. J. Müller, F. Finger, R. Carius, and H. Wagner, Phys. Rev. B **60**, 11666 (1999).

34. C. Malten, F. Finger, J. Müller, and S. Yamasaki, Mater. Res. Soc. Symp. Proc. **507**, 757 (1998).

35. B. I. Shklovskii, H. Fritzsche, and S. D. Baranovskii, Phys. Rev. Lett. **62**, 2989 (1989); E. I. Levin, S. Marianer, and B. I. Shklovskii, Phys. Rev. B**45**, 5906 (1992).

36. See, for example, R. A. Street, *Hydrogenated Amorphous Silicon* (Cambridge University Press, Cambridge, 1991).

37. B. Yan, N. A. Schultz, A. L. Efros, and P. C. Taylor, Phys. Rev. Lett. **84**, 4180 (2000).

38. B. Yan and P. C. Taylor, MRS Symp. Proc. **507**, 805 (1998).

39. T. Su, S. Chen, P. C. Taylor, R. S. Crandall, and A. H. Mahan, Phys. Rev. B **62**, 12849 (2000).

40. T. Su, R. Plachy, and P. C. Taylor, J. Non-Cryst. Solids (2002), in press.

41. R. A. Street and D. K. Biegelsen, Solid State Commun. **33**, 1159 (1980); R. A. Street and D. K. Biegelsen, Solid State Commun. **44**, 501 (1982).

42. N. Shultz, B. Yan, A. L. Efros, and P.C. Taylor, J. Non-Cryst. Solids **266-269**, 372-375 (2000).

43. J. Whitaker, T. Su, and P.C. Taylor, Mat. Res. Soc. Symp. Proc. **715**, A2.4 (2002).

44. R.A. Street, *Hydrogenated Amorphou*s Silicon (Cambridge University Press, Cambridge, 1991).

45. H. Dersch, J. Stuke, and J. Beichler, Appl. Phys. Lett. **38** (1980) 456.

46. P.V. Santos, C. F. de O. Graeff, and I. Chambouleyron, J. Non-Cryst. Solids **128** (1991) 243.

47. K. Eberhardt and G. H. Bauer, J. Non-Cryst. Solids **164-166** (1993) 19-22.

48. T. Unold, Mat. Res. Soc. Proc. **336** (1994) 287.

49. H. Fritzsche, P. Stradins, and G. Belomoin, Mat. Res. Soc. Symp. Proc. **520** (1996) 563.

50. J.D. Cohen, Solar Energy Mat. and Solar Cells **78** (2003) 399.

51. F. C. Marques, M. M. de Lima, Jr., and P. C. Taylor, Appl. Phys. Lett. **74** (1999) 3797; J. Non-Cryst. Solids **299-302** (2002) 571.

52. M Stutzmann, W. B. Jackson, and C. C. Tsai, Phys. Rev. B**32** (1985) 23.

53. D. Redfield, Appl. Phys. Lett. **54** (1989) 398.

54. S. Nitta, YU. Takahashi, and M. Noda, J. de Phys. **42** (1981) C4-403.

55. N. Schultz and P. C. Taylor, MRS Symp. Proc. **609** (2001) A3.4.1.

56. G. Schumm, E. Lotter, and G.H. Bauer, Appl. Phys. Lett. **60**, p. 3262 (1992).

57. G. Ganguly, S. Yamasaki, and A. Matsuda, Phil. Mag. B **63**(1) p. 281 (1991).

58. M. Gunes and C.R. Wronski, J. Appl. Phys. **81**, p. 3526 (1997).

59. J. Pearce, X. Niu, R. Koval, G. Ganguly, D. Carlson, R.W. Collins, C.R. Wronski, Mat. Res. Soc. Proc., **664**, A12.3 (2001).

60. D. Han and H. Fritzsche, J. Non-Cryst. Solids, **59-60**, p. 397 (1983).

61. P. Stradins and H. Fritzsche, Philos. Mag. B **69**, p.121 (1994).

62. L. Yang, L. Chen, and A. Catalano, Appl. Phys. Lett. **59**, p. 840 (1991).

63. X. Xu, J. Yang, and S. Guha, Mat. Res. Soc. Proc., **297** 649 (1993).

64. J. M. Pearce, R. J. Koval, X. Niu, S. J. May, R.W. Collins, and C. R. Wronski, , 17th European Photovoltaic Solar Energy Conference Proceedings, **3**, pp. 2842-2845 (2002).

65. J. M. Pearce, J. Deng, R. W. Collins, and C. R. Wronski, Appl. Phys. Lett., **83**(18), pp. 3725-3727 (2003).

66. J. M. Pearce, J. Deng, V. Vlahos, R. W. Collins, and C. R. Wronski, "Light Induced Changes in Two Distinct Defect States At and Below Midgap in a-Si:H", Proceedings of the 3rd World Conference on Photovoltaic Energy Conversion, (in press).

67. C. R. Wronski, R. W. Collins, V. Vlahos, J. M. Pearce, J. Deng, M. Albert, G. M. Ferreira, and C. Chen, "Optimization of Phase-Engineered a-Si:H-Based Multijunction Solar Cells", *National Renewable Energy Laboratory Annual Report,* Contract #: NDJ-2-30630-01, (2004).

68. P.C. Taylor and W. D. Ohlsen, Solar Cells, **9** pp. 113-118 (1983).

69. H. Fritzsche, Ann. Rev. Mater. Res. **31**, 47 (2001).

70. S. Zukotynski, F. Gaspari, N. Kherani, T. Kosteski, K. Law, W.T. Shmayda, C.M. Tan, J. Non-Cryst. Solids **299-302,** 476 (2002).

71. W. B. Jackson and N. B. Amer, Phys. Rev. B. **25**, 5559 (1982).

10. PUBLICATIONS

1. "Microscopic Nature of the Er^{3+} Emission in Mixed Amorphous-Nanocrystalline Si:H Films (S. B. Aldabergenova, P. C. Taylor, H. P. Strunk, and A. A. Andreev), J. Appl. Phys. **90**, 2773 (2001).

2. "Structural Characterization of SiF_4, SiH_4, and H_2 Hot-Wire-Grown Microcrystalline Silicon Thin Films with Large Grains" (J. J. Gutierrez, C. E. Inglefield, C. P. An, M. C. DeLong, P. C. Taylor, S. Morrison, and A. Madan), MRS Symp. Proc. **664** A3.4.1 (2001).

3. "Universal Distribution of Optically Excited Carriers in Tetrahedral Amorphous Semiconductors" (N. A. Schultz, B. Yan, A. L. Efros, and P. C. Taylor), J. Non-Cryst. Solids **299-302**, 300 (2002).

4. "NMR Probe of Band Tail States in a-Si:H" (T. Su, R. Plachy, P. C. Taylor, and P. Hari), J. Non-Cryst. Solids **299-302**, 589 (2002).

5. "On the Interpretation of Paramagnetic Centers in Intrinsic Hydrogenated Microcrystalline Silicon" (M. M. De Lima, Jr., S. Morrison, A. LeGeune, F. C. Marques, and P. C. Taylor), J. Non-Cryst. Solids **299-302**, (2002).

6. "Defect Transition Energies and the Density of Electronic States in Hydrogenated Amorphous Silicon" (G. Mensing, J. M. Gilligan, P. Hari, P. C. Taylor, E. Hurt, G. Lupke, S. T. Pantelides, and N. H. Tolk), J. Non-Cryst. Solids **299-302**, 621 (2002).

7. "Recombination Mechanism of Residual Electrons in Amorphous Hydrogenated Germanium after Light Excitation" (F. C. Marques, M. M. De Lima, Jr., and P. C. Taylor), J. Non-Cryst. Solids **299-302**, 571 (2002).

8. "Recombination of Optically Excited Carriers in a-Si:H at Low Temperatures and Intermediate Times" (J. Whitaker, T. Su, and P. C. Taylor), MRS Symp. Proc. **715**, 275 (2002).

9. "^{1}H NMR Evidence for a Change in the Local Hydrogen Environment of Sites Associated with the Staebler-Wronski Effect in a-Si:H" (T. Su, R. Plachy, P. C. Taylor, S. Stone, G. Ganguly, and D. E. Carlson), MRS Symp. Proc. **715**, 423 (2002).

10. "Light-Induced Degradation in Solar Cells with Hydrogenated Amorphous Silicon-Sulfur Active Layers" (W. Xu and P. C. Taylor), MRS Symp. Proc. **715**, 435 (2002).

11. "Magnetic Resonance Probes of Band Tail States and Defects in Tetrahedrally Coordinated Amorphous Semiconductors" (P. C. Taylor), MRS Symp. Proc. **715**, 257 (2002).

12. "Paramagnetic Centers in Microcrystalline Silicon" (M. M. De Lima, Jr., S. Morrison, A. LeGeune, F. C. Marques, and P. C. Taylor), MRS Symp. Proc. **715**, 321 (2002).

13. "ESR Observations of Paramagnetic Centers in Intrinsic Microcrystalline Silicon" (M. M. De Lima, Jr., S. Morrison, A. LeGeune, F. C. Marques, and P. C. Taylor), Phys. Rev. B**65**, 235324-1 (2002).

14. "Low Temperature, Light Induced Production of Silicon Dangling Bonds in Hydrogenated Amorphous Silicon" (N. A. Schultz and P. C. Taylor), Phys Rev. B**65**, 235207-1 (2002).

15. "The Direct Role of Hydrogen in the Staebler-Wronski Effect in Hydrogenated Amorphous Silicon" (T. Su, P. C. Taylor, D. E. Carlson, and G. Ganguly), Phys. Rev. Lett. **89**, 15502-1 (2002).

16. "Temperature Dependence of the Decay of Optically Excited Charge Carriers in Amorphous Silicon" (J Whitaker and P. C. Taylor), MRS Symp. Proc. **762**, 63 (2003).

17. "Temperature Dependence of a Hydrogen Doublet Site in Light-Soaked a-Si:H from ^{1}H NMR" (T. Su, P. C. Taylor, G. Ganguly, and D. E. Carlson), MRS Symp. Proc. **762**, 27 (2003).

18. "A Hydrogen-Related Defect And The Staebler-Wronski Effect In Hydrogenated Amorphous Silicon" (T. Su, P. C. Taylor, G. Ganguly, and D. E. Carlson), J. Non-Cryst. Solids **338-340**, 357(2004).

19. "The Staebler-Wronski Effect In Amorphous Germanium" (J. Whitaker, P. C. Taylor, M.M. de Lima Jr., and F.C. Marques), J. Non. Cryst. Solids **338-340**, 374 (2004).

20. "The Staebler-Wronski Effect in Hydrogenated Amorphous Germanium" (J. Whitaker, P. C. Taylor, M. M. de Lima and F. Marques), Phys. Rev. B (2005), submitted.

21. "Tritium Induced Defects in Amorphous Silicon" (J . Whitaker, J. Viner, P. C. Taylor, S. Zukotynski, E. Johnson, and P. Stradins, MRS Symp. Proc. **808,** 159 (2004).

22. "Evolution of D^0 and non-D^0 Light Induced Defect States in a-Si:H Materials and Their Respective Contributions to Carrier Recombination" (J. M. Pearce, V. Vlahos, J. Deng, R. W. Collins, C. R. Wronski, J. Whitaker, and P. C. Taylor), MRS Symp. Proc. **808**, 153 (2004).

23. "Studies of SiH_2 and its Potential Role in Light-Induced Metastability in Amorphous Silicon Hydride" (with T. A. Abtew, D. A. Drabold, and P. C. Taylor), Appl. Phys. Lett. (2005), submitted.

REPORT DOCUMENTATION PAGE

Form Approved
OMB No. 0704-0188

1. REPORT DATE *(DD-MM-YYYY)* November 2005	2. REPORT TYPE Subcontract Report	3. DATES COVERED *(From - To)* 15 December 2001–31 January 2005

4. TITLE AND SUBTITLE	5a. CONTRACT NUMBER
Characterization of Amorphous Silicon Advanced Materials and PV Devices: Final Technical Report, 15 December 2001–31 January 2005	DE-AC36-99-GO10337

5b. GRANT NUMBER

5c. PROGRAM ELEMENT NUMBER

6. AUTHOR(S)	5d. PROJECT NUMBER
P.C. Taylor	NREL/SR-520-38678

5e. TASK NUMBER
PVB65101

5f. WORK UNIT NUMBER

7. PERFORMING ORGANIZATION NAME(S) AND ADDRESS(ES)	8. PERFORMING ORGANIZATION REPORT NUMBER
Department of Physics University of Utah Salt Lake City, UT 84112	ADJ-2-30630-23

9. SPONSORING/MONITORING AGENCY NAME(S) AND ADDRESS(ES)	10. SPONSOR/MONITOR'S ACRONYM(S)
National Renewable Energy Laboratory 1617 Cole Blvd. Golden, CO 80401-3393	NREL

11. SPONSORING/MONITORING AGENCY REPORT NUMBER
NREL/SR-520-38678

12. DISTRIBUTION AVAILABILITY STATEMENT
National Technical Information Service
U.S. Department of Commerce
5285 Port Royal Road
Springfield, VA 22161

13. SUPPLEMENTARY NOTES
NREL Technical Monitor: Bolko von Roedern

14. ABSTRACT *(Maximum 200 Words)*
The major objectives of this subcontract have been: (1) understand the microscopic properties of the defects that contribute to the Staebler-Wronski effect to eliminate this effect, (2) perform correlated studies on films and devices made by novel techniques, especially those with promise to improve stability or deposition rates, (3) understand the structural, electronic, and optical properties of films of hydrogenated amorphous silicon (a-Si:H) made on the boundary between the amorphous and microcrystalline phases, (4) search for more stable intrinsic layers of a-Si:H, (5) characterize the important defects, impurities, and metastabilities in the bulk and at surfaces and interfaces in a-Si:H films and devices and in important alloy systems, and (6) make state-of-the-art plasma-enhanced chemical vapor deposition (PECVD) devices out of new, advanced materials, when appropriate. All of these goals are highly relevant to improving photovoltaic devices based on a-Si:H and related alloys. With regard to the first objective, we have identified a paired hydrogen site that may be the defect that stabilizes the silicon dangling bonds formed in the Staebler-Wronski effect.

15. SUBJECT TERMS
PV; module; amorphous silicon; advanced materials; Staebler-Wronski effect; plasma-enhanced chemical vapor deposition (PECVD); devices; photoconductivity;

16. SECURITY CLASSIFICATION OF:			17. LIMITATION OF ABSTRACT	18. NUMBER OF PAGES	19a. NAME OF RESPONSIBLE PERSON
a. REPORT Unclassified	b. ABSTRACT Unclassified	c. THIS PAGE Unclassified	UL		
					19b. TELEPONE NUMBER *(Include area code)*

Standard Form 298 (Rev. 8/98)
Prescribed by ANSI Std. Z39.18

F1146-E(05/2004)